UNIVERSIDADE
BEIRA INTERIOR

# Development of gold core silica shell nanospheres for cancer therapy

**Rafaela da Silva Guimarães**

Dissertação para obtenção do Grau de Mestre em
**Ciências Biomédicas**
(2º ciclo de estudos)

Orientador: Prof. Doutor Ilídio Joaquim Sobreira Correia
Co-orientador: Doutor André Ferreira Moreira
Mestre Ana Carolina Félix Rodrigues

**setembro de 2020**

*“Je connais mes limites. C’est pourquoi je vais au-delà.”*

-Serge Gainsbourg

À minha mãe, avó e avô por tudo o que sempre fizeram por mim…

# Acknowledgments

Primeiro, quero agradecer ao meu orientador, professor Ilídio Correia, pela oportunidade que me deu de trabalhar neste projeto e de me ter deixado integrar neste grupo. Agradecer também por todos os ensinamentos e por toda a exigência, que me fizeram melhorar tanto a nível profissional como pessoal.

Depois, quero também agradecer aos meus co-orientadores, André Moreira e Carolina Rodrigues, a quem estou profundamente grata por toda a disponibilidade, paciência e tempo despendido para me ajudarem ao longo deste ano. Também agradeço por toda a boa disposição e por todos os esclarecimentos das minhas dúvidas que por vezes sei que eram difíceis de perceber. Sem o apoio e orientação dado ao longo deste trabalho não teria sido possível concretizá-lo.

Um obrigado também ao Duarte por sempre me ajudar quando eu precisei. E também à Rita, Cátia e Sol pelo seu apoio e por estarem sempre prontas a ajudar. À Ariana e ao Nata, meus colegas de trabalho, porque mesmo eu tendo mau feitio souberam lidar comigo com paciência. Obrigada por todo o apoio que me deram. Aos restantes colegas, e apesar de nos conhecermos há pouco tempo, gostaria de agradecer o apoio e incentivo.

A todos os meus outros amigos, desde aqueles que já estão comigo há bastantes anos, mas também aos que surgiram ao longo destes últimos 5 anos em que estive na universidade, que me conhecem bem e que sabem que por mais ocupada que esteja tento arranjar sempre um tempo para eles. Por toda a paciência que tiveram com as minhas crises, por todo o incentivo, força, por tudo o que fizeram para me animar e para conseguir espairecer quando mais precisava.

Por fim, um grande obrigada à minha mãe e à minha avó por tudo o que fizeram para me ajudar e porque me incentivaram a nunca desistir. Ensinaram-me a nunca baixar os braços por mais difícil que a vida possa ser, por todo o carinho e por me ajudarem em tudo o que podiam. Ao meu avô, que só esteve presente em parte desta jornada, mas que foi e será sempre importante na minha vida. Todo o apoio e carinho que ele sempre me deu foi e continuará a ser importante para toda a minha vida. A eles estou eternamente grata por tudo o que fizeram, um obrigada não é suficiente para agradecer por tudo.

# Resumo

Atualmente o cancro é um dos principais problemas de saúde pública, apresentando uma elevada incidência e taxa de mortalidade crescente na população mundial. Entre as opções de tratamento disponíveis, a quimioterapia é a terapia anticancerígena mais comummente aplicada na clínica, contudo apresenta uma baixa eficácia terapêutica. Este cenário é explicado pela rápida degradação, reduzida solubilidade e seletividade dos fármacos quimioterapêuticos usados em meio clínico para eliminar as células cancerígenas. Por outro lado, as células cancerígenas têm a capacidade de desenvolver resistência a múltiplos fármacos, o que reforça a necessidade de desenvolver abordagens terapêuticas mais eficazes. Assim sendo, as terapias combinatórias baseadas na administração simultânea de múltiplos fármacos surgem como uma abordagem promissora, uma vez que a combinação de fármacos pode levar a um efeito terapêutico sinérgico, incrementando a eficácia da quimioterapia. Além disso, as terapias combinatórias possibilitam a redução das doses dos fármacos administrados, minimizando assim os seus efeitos colaterais. Contudo, os fármacos quimioterapêuticos apresentam limitações que condicionam a sua administração intravenosa. Assim, a par da necessidade de desenvolver novas combinações de medicamentos com alto potencial terapêutico, é crucial desenvolver sistemas de entrega capazes de aumentar a seletividade, eficácia terapêutica, e ainda reduzir a sua toxicidade sistémica. Dentro dos sistemas de entrega de fármacos que tem vindo a ser desenvolvidos destacam-se as nanopartículas de ouro com revestimento de sílica (AuMSS). Estes nanosistemas apresentam propriedades físico-químicas e biológicas que permitem a sua aplicação não só como transportadores dos agentes terapêuticos, mas também como agentes de imagiologia.

O trabalho de investigação desenvolvido durante o meu 2 º ano de mestrado teve como objetivo desenvolver uma nova combinação de fármacos à base de doxorrubicina (DOX) e laranja de Acridina (AO) para ser entregue a células cancerígenas por AuMSS esféricas. Por outro lado, foi ainda desenvolvido um revestimento de superfície baseado em Polietilenoglicol (PEG) e Anisamida (ANIS) com o intuito de aumentar o tempo de circulação na corrente sanguínea e a seletividade do nanosistema para as células cancerígenas. A ANIS foi selecionada devido à sua especificidade para os recetores sigma que estão sobreexpressos em alguns dos tipos de cancro. Por outro lado, o PEG foi selecionado devido à sua natureza anfifílica e elevada solubilidade, o que permite reduzir a adsorção de proteínas na superfície das nanopartículas, e consequentemente aumentar

o seu tempo de circulação na corrente sanguínea. Os resultados obtidos neste estudo demonstraram que a combinação DOX:AO pode mediar um efeito terapêutico sinérgico tanto em células cancerígenas do colo do útero (HeLa) como em células do cancro da mama (MCF-7), principalmente quando são usados rácios 2:1, 1:1 e 1:2. A funcionalização das AuMSS com PEG e ANIS (AuMSS-TPANIS) resultou num aumento do tamanho médio destes nanosistemas (para 190 nm), mas também lhes conferiu uma maior estabilidade coloidal. O sucesso da ligação dos polímeros às nanopartículas foi ainda confirmado por análise termogravimétrica (TGA) e por espectroscopia de infravermelho por transformada de Fourier (FTIR). Nos estudos *in vitro,* as nanopartículas mostraram ser biocompatíveis quando em contacto com células saudáveis (fibroblastos) e células cancerígenas (HeLa e MCF-7) até à máxima concentração testada de 200 μg/mL. Verificou-se ainda que a funcionalização das nanopartículas com ANIS aumentou a sua internalização pelas células MCF-7 (linha celular que sobreexpressa os recetores sigma). Esta maior seletividade para as células MCF-7 traduziu-se também num maior efeito citotóxico nestas células cancerígenas, quando comparado com o observado nas células HeLa.

Em suma, os resultados apresentados confirmam a funcionalização das nanopartículas com o PEG e ANIS, o potencial terapêutico da combinação DOX:AO e ainda a capacidade de direcionamento para as células cancerígenas das AuMSS-TPANIS.

# Palavras-chave

Cancro;combinação de fármacos;doxorrubicina;laranja de acridina;nanopartículas de núcleo de ouro com revestimento de sílica;PEG;anisamida.

# Resumo alargado

Atualmente o cancro é um dos principais problemas de saúde pública, apresentando uma elevada incidência e taxa de mortalidade crescente na população mundial. Os tratamentos convencionais como a quimioterapia, radioterapia e cirurgia caracterizam-se por apresentar uma baixa eficácia terapêutica estando associados a diversos efeitos secundários. Entre os tratamentos disponíveis, a quimioterapia é o tratamento mais utilizado na clínica, apesar das suas diversas limitações. Os agentes quimioterapêuticos são facilmente degradados e caracterizam-se por possuírem uma baixa solubilidade, biodisponibilidade e seletividade para o tumor, o que consequentemente potencia diversos efeitos secundários. Por outro lado, as células cancerígenas têm a capacidade de adquirir um fenótipo de resistência a múltiplos fármacos o que limita ainda mais a eficácia terapêutica da quimioterapia. De forma a ultrapassar estas limitações novas abordagens envolvendo a combinação de fármacos têm vindo a ser desenvolvidas. As terapias combinatórias baseadas na administração simultânea de dois ou mais fármacos surgem como uma solução promissora, uma vez que a combinação de agentes terapêuticos que apresentam mecanismos de ação diferentes pode levar a um efeito terapêutico sinérgico, incrementando a eficácia terapêutica da quimioterapia. Além disto as terapias combinatórias possibilitam a redução das doses dos fármacos administrados, minimizando assim os seus efeitos colaterais. Apesar do potencial deste tipo de abordagem, a combinação de múltiplos fármacos apresenta limitações que condicionam a sua administração intravenosa. A ocorrência de efeitos antagonistas e a presença de diferentes perfis farmacocinéticos podem levar a uma diminuição da eficácia antitumoral da terapia combinatória. Desta forma, a par da necessidade de desenvolver novas combinações de medicamentos com alto potencial terapêutico, é crucial desenvolver sistemas de entrega capazes de aumentar a seletividade e eficácia terapêutica dos fármacos, e simultaneamente reduzir a sua toxicidade sistémica. Os avanços na área da nanotecnologia permitiram desenvolver sistemas à escala nanométrica (nanopartículas) com capacidade de superar as limitações associadas à quimioterapia. Estes nanosistemas possuem a capacidade de encapsular fármacos, prevenindo a sua degradação e libertação prematura e permitindo ainda o seu direcionamento específico para as células cancerígenas. Dentro dos sistemas de entrega de fármacos em desenvolvimento para aplicação na terapia do cancro, destacam-se as nanopartículas de ouro com revestimento de sílica (AuMSS), que devido às suas propriedades físico-químicas e biológicas permitem não só a sua aplicação como transportadores dos agentes terapêuticos mas também como agentes de imagiologia. Nestes sistemas, o núcleo de ouro funciona como

agente de contraste para a realização de exames imagiológicos e a camada de sílica mesoporosa permite a encapsulação de diferentes agentes terapêuticos. Contudo, a aplicação destas nanopartículas na terapia do cancro pode ser dificultada devido à sua reduzida biodisponibilidade e especificidade para as células cancerígenas.

Desta forma, o trabalho de investigação desenvolvido durante o meu 2 º ano de mestrado teve objetivo desenvolver uma nova combinação de fármacos à base de doxorrubicina (DOX) e laranja de Acridina (AO) para ser entregue a células cancerígenas por AuMSS esféricas. A DOX é um fármaco amplamente utilizado no tratamento de diferentes tipos de cancro, exercendo o seu efeito através da inibição da topoisomerase II e pela sua intercalação nas cadeias de DNA. Por seu lado, a AO é um corante que possuiu acumulação preferencial em microambientes acídicos (p.ex. cancro), conseguindo também este intercalar-se na dupla cadeia de DNA. Adicionalmente, também foi desenvolvido um revestimento de superfície baseado em Polietilenoglicol (PEG) e Anisamida (ANIS) com o intuito de aumentar o tempo de circulação na corrente sanguínea e a seletividade do nanosistema para as células cancerígenas. A ANIS foi selecionada devido à sua especificidade para os recetores sigma que estão sobreexpressos nas membranas das células cancerígenas. Por outro lado, o PEG foi selecionado devido à sua natureza anfifílica e elevada solubilidade, o que permite reduzir a adsorção de proteínas na superfície das nanopartículas, e consequentemente aumentar o seu tempo de circulação na corrente sanguínea.

O potencial terapêutico da combinação DOX:AO foi avaliado em células cancerígenas do cancro da mama (MCF-7) e do cancro do colo do útero (HeLa) explorando diferentes rácios molares (5:1 a 1:5) de combinação dos fármacos. Os resultados obtidos demonstraram que a combinação DOX:AO pode mediar um efeito terapêutico sinérgico tanto em células HeLa como em células MCF-7, principalmente quando são usados rácios 2:1, 1:1 e 1:2. Por outro lado, a funcionalização das AuMSS com PEG e ANIS (AuMSS-TPANIS) resultou na formação de nanopartículas com um tamanho médio de 190 nm e carga de superfície negativa ≈-20 mV. Adicionalmente, a introdução do PEG na superfície das AuMSS também conferiu uma maior estabilidade coloidal ao nanosistema. O sucesso da ligação dos polímeros às nanopartículas foi ainda confirmado por análise termogravimétrica (24% de conteúdo polimérico) e por espectroscopia de infravermelho por transformada de Fourier (FTIR). Nos estudos *in vitro,* as nanopartículas mostraram ser biocompatíveis quando em contacto com células saudáveis (fibroblastos) e células cancerígenas (HeLa e MCF-7) até à máxima concentração testada de 200 μg/mL. Verificou-se ainda que a funcionalização das AuMSS com PEG e ANIS aumentou a sua internalização pelas células MCF-7 (linha

celular que sobreexpressa os recetores sigma) em ≈300% quando comparadas com as partículas não revestidas. Esta maior seletividade para as células MCF-7 traduziu-se também num maior efeito citotóxico, reduzindo a viabilidade destas células para ≈40% enquanto que as células HeLa apresentaram valores de viabilidade celular perto de 90%.

Em suma, os resultados apresentados confirmam a funcionalização das nanopartículas com o PEG e ANIS, o potencial terapêutico da combinação DOX:AO e ainda a capacidade de direcionamento para as células cancerígenas das AuMSS-TPANIS.

# Abstract

Currently, cancer is major public health problem, presenting an increasing incidence and mortality rate that affects the worldwide population. Among the treatments used in the clinic, chemotherapy is the most commonly used anticancer therapy, despite its low therapeutic efficacy. This scenario can be explained by rapid degradation, reduced solubility, and selectivity of chemotherapeutic drugs to cancer cells. Additionally, cancer cells can develop resistance to multiple drugs, which highlights the necessity to develop novel and more effective anti-cancer approaches. Combinatorial therapies based on the simultaneous administration of multiple drugs can lead to synergistic effects, which consequently increase the therapeutic efficiency of chemotherapy. However, chemotherapeutic drugs present limitations that impair their intravenous administration. Thus, despite the need to found novel drug combinations with high therapeutic potential, it is crucial to develop delivery systems capable of increasing the drugs' therapeutic selectivity and efficacy while simultaneously decreasing their systemic toxicity. Among the drug delivery systems that have been developed so far, gold core silica shell (AuMSS) nanoparticles present excellent physicochemical and biological properties that allow their simultaneous application in chemotherapy and bioimaging. Thus, the research work developed during the second year of my master's degree aimed to design a dual drug combination based on Doxorubicin (DOX) and Acridine orange (AO) to be encapsulated in AuMSS nanospheres. Moreover, a novel AuMSS surface modification using 3-(Triethoxysilyl)propyl isocyanate-Poly(ethylene glycol)-4-Methoxybenzamide (TPANIS) was developed to improve nanoparticles' blood circulation time and specificity to cancer cells. The 4-Methoxybenzamide or Anisamide (ANIS) was selected due to its specificity for sigma receptors that are overexpressed in the cancer cells' membranes. On the other hand, PEG was selected due to its amphiphilic nature and high solubility, that lead to a reduce protein adsorption on nanoparticles' surface, and consequently increase its blood circulation time.

The obtained results demonstrated that the DOX:AO drug combination can mediate a synergistic therapeutic effect in both HeLa and MCF-7 cells, particularly at the 2:1, 1:1, and 1:2 ratios. Otherwise, AuMSS nanoparticles' functionalization with the TPANIS promoted a slight increase in the nanoparticles' size and stability. The successful incorporation of the polymers on nanoparticles surface was also confirmed by thermogravimetric analysis (TGA) and by Fourier Transform Infrared Spectroscopy (FTIR). Additionally, both the DOX and AO were successfully encapsulated on the

AuMSS-TPANIS nanospheres. In *in vitro* studies, nanoparticles demonstrated to be biocompatible when in contact with healthy cells (fibroblasts) and cancer cells (HeLa and MCF-7) up to the maximum tested concentration of 200 μg/mL. Moreover, the AuMSS nanospheres' functionalization with TPANIS significantly increased their internalization by MCF-7 cells. This selectivity towards MCF-7 (overexpressing sigma receptors) also resulted in an enhanced cytotoxic effect against this cell line.

In summary, the presented results confirm the successful functionalization of AuMSS nanoparticles with PEG and ANIS. Additionally, the therapeutic potential of the DOX:AO drug combination as well as the targeting capacity of AuMSS-TPANIS nanospheres were also demonstrated. Such supports the application of AuMSS-TPANIS nanoparticles for cancer-targeted chemotherapy based on the DOX:AO drug combination.

# Keywords

Cancer, drugs combination, acridine orange, doxorubicin, gold core silica shell nanoparticles, PEG, anisamide.

# List of Publications

### Article published in a peer-reviewed journal:

Rafaela S. Guimarães, Carolina F. Rodrigues, André F. Moreira and Ilídio J. Correia, (2020), "Overview of stimuli-responsive mesoporous organosilica nanocarriers for drug delivery". *Pharmacological Research*. 155: 104742. DOI: 10.1016/j.phrs.2020.104742.

# Index

# Table Index

# Figure Index

# List of Abbreviations

| | |
|---|---|
| AO | Acridine Orange |
| ANIS | 4-Methoxybenzamide or Anisamide |
| ATP | Adenosine Triphosphate |
| AuMSS | Gold Core Silica Shell Nanoparticles |
| AuMSS-TPANIS | AuMSS with TPANIS |
| Bcl-2 | B-cell Lymphoma 2 |
| CDI | 1,1′-Carbonyldiimidazole |
| CI | Combination Index |
| CT | Computerized Tomography |
| CTAB | Hexadecyltrimethylammonium Bromide |
| DCM | Dichloromethane |
| DDS | Drug or Gene Delivery Systems |
| DLS | Dynamic Light Scattering |
| DMEM-HG | Dulbecco's Modified Eagle Medium-High Glucose |
| DMEM-F12 | Dulbecco's Modified Eagle Medium F-12 |
| DNA | Deoxyribonucleic Acid |
| DOX | Doxorubicin Hydrochloride |
| DOX:AO | Doxorubicin: Acridine Orange |
| ECM | Extracellular Matrix |
| E.E | Encapsulation Efficiency |
| EPR | Enhanced Permeability and Retention |
| EtOH | Ethanol |
| FibH | Primary Normal Human Dermal Fibroblasts |
| FITC | Fluorescein Isothiocyanate |
| FTIR | Fourier Transform Infrared Spectroscopy |
| GSH | Disulfide Glutathione |
| $HAuCl_4$ | Hydrogen Tetrachloroaurate (III) Hydrate |
| HCl | Hydrochloric Acid |
| HeLa | Human Negroid Cervix Epithelioid Carcinoma |
| HU | Hounsfield Units |
| ICs | Inhibitory Concentrations |
| IC20 | 20% Maximal Inhibitory Concentration |
| IC50 | Half Maximal Inhibitory Concentration |

| | |
|---|---|
| IC80 | 80% Maximal Inhibitory Concentration |
| KRB | Krebs Ringer Buffer |
| $K^-$ | Negative Control |
| $K^+$ | Positive Control |
| MCF-7 | Michigan Cancer Foundation-7 |
| MDR | Multidrug Resistance |
| MetOH | Methanol |
| MRI | Magnetic Resonance Imaging |
| NADH | Nicotinamide Adenine Dinucleotide |
| NaOH | Sodium Hydroxide |
| NIR | Near-infrared |
| ns | Non-significant |
| PA | Photoacoustic |
| PANIS | PEG Linked to ANIS |
| PBS | Phosphate Buffered Saline |
| PDI | Polydispersity Index |
| PDT | Photodynamic Therapy |
| PEG | Poly(ethylene glycol) |
| PEOZ | Poly-2-ethyl-2-oxazoline |
| P-gp | P-glycoprotein |
| PHEMA | Poly(2-hydroxyethyl methacrylate) |
| PTT | Photothermal Therapy |
| pRb | Retinoblastoma Protein |
| RBCs | Red Blood Cells |
| RES | Reticuloendothelial System |
| RGD | Arginylglycylaspartic Acid |
| RNA | Ribonucleic Acid |
| ROS | Reactive Species of Oxygen |
| SERS | Surface-enhanced Raman Spectroscopy |
| s.d. | Standard Deviation |
| SPR | Surface Plasmon Resonance |
| TEM | Transmission Electron Microscopy |
| TEOS | Tetraethyl Orthosilicate |
| TESPIC | 3-(Triethoxysilyl)propyl Isocyanate |
| TGA | Thermogravimetric Analysis |
| THF | Tetrahydrofuran |
| Top II | Topoisomerase II |

| | |
|---|---|
| TPANIS | PANIS Modified with TESPIC or 3-(Triethoxysilyl)propyl isocyanate-poly(ethylene glycol)-4-methoxybenzamide |
| TSP-1 | Thrombospondin-1 |
| UK | United Kingdom |
| USA | United States of America |
| UV-vis | Ultraviolet-visible |
| VEGF-A | Vascular Endothelial Growth Factor-A |
| β-CD | Beta-cyclodextrin |

# Chapter 1

# Introduction

# 1. Introduction

## 1.1. Cancer

### 1.1.1. Cancer epidemiology

Cancer is a leading health problem worldwide and is responsible for millions of deaths every year [1]. In 2018, cancer incidence and mortality increased around the world, reaching 18.1 million new cases and a mortality rate of 9.6 million cases per year [2]. In the current year, in the United States of America (USA) is estimated that will occur 1 806 590 new cancer cases and 606 520 cancer-related deaths. Relatively to the new cancer cases in the USA for 2020, the most common types of cancers that are expected to be diagnosed in men are prostate (21%) and lung & bronchus (13%), whereas the breast (30%) and lung & bronchus (12%) cancers should be the most prevalent in women [3]. In Portugal, according to *Direção Geral de Saúde*, the cancer incidence should continue to increase at a rate of 3% per year. Further, it is projected that will occur 60 000 new cases of cancer and 30 000 cancer-related deaths in 2035 [4].

Several factors can be associated with cancer development, such as environmental, genetic, social, hormonal, and lifestyle conditions. In the latter, the smoking, reduced physical activity, and ingestion of highly processed food rich in calories are linked to an increased probability of developing cancer [5].

### 1.1.2. Cancer development and treatments approaches

Cancer is a group of diseases characterized by the uncontrolled proliferation of cells, which can invade and spread via the lymphatic system to distant parts of the body [6]. The cancer tissue is comprised of the cancer cells, blood vessels, fibroblasts, macrophages, lymphocytes, and different cells that are incorporated into an extracellular matrix (ECM) and an interstitial fluid [7-9]. The increased complexity of the tumor microenvironment and the crosstalk between the different elements is paramount for cancer development [10, 11]. Additionally, most of the tumors present a high cellular and ECM density, which difficult the diffusion of molecules (*e.g.* nutrients, metabolites, and therapeutic agents) and gases to the interior regions of this tissue [12]. Such fact also impacts on the development of the cells within the tumors, which can be organized in three different regions, i) the proliferative zone, outer region of cells rich in nutrients and oxygen; ii) the non-proliferative zone, an intermediary region of cells with reduced access to nutrients and oxygen; and iii) the necrotic zone, a deeper region of the tumor composed by necrotic cells due to the limited access to nutrients and oxygen as well as the accumulation of metabolites (*e.g.* lactate) [13, 14].

Otherwise, Hanahan and Weinberg identified several key characteristics, *i.e.* hallmarks of cancer, that support the cancer cells' establishment, survival, and growth (Figure 1) [15].

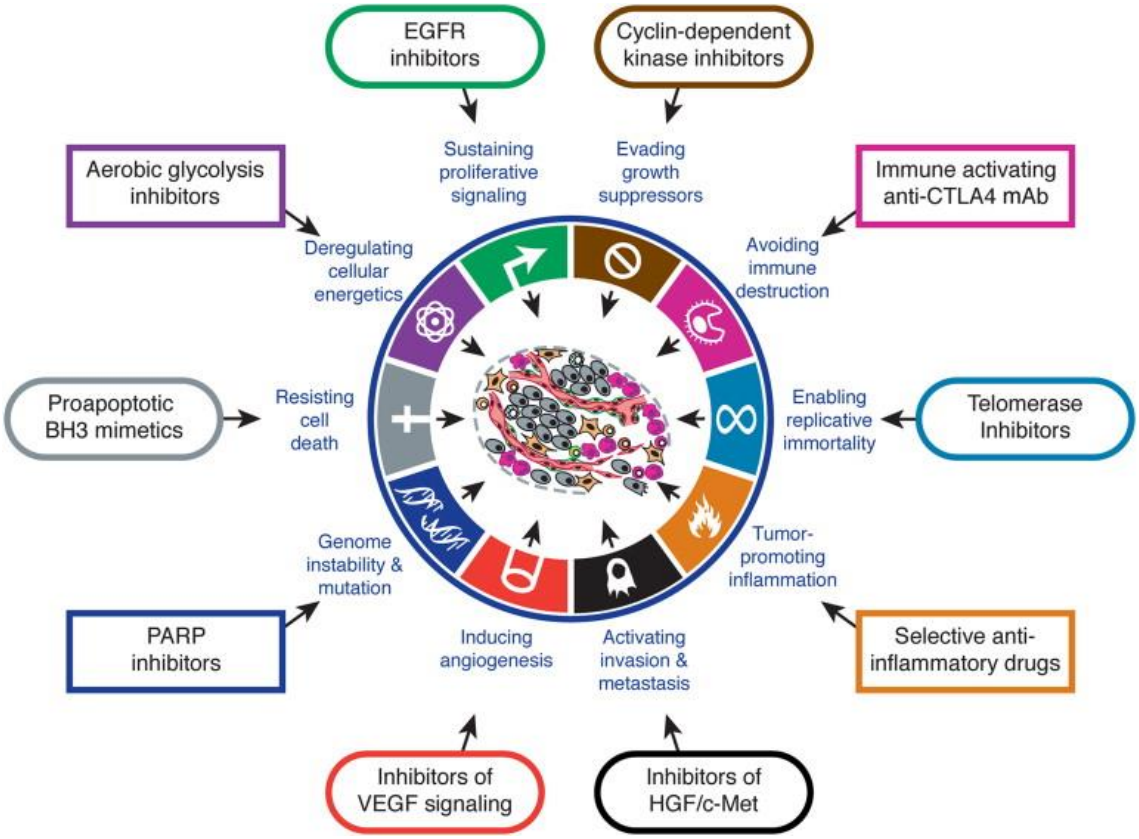


**Figure 1** - Hallmarks of cancer cells and examples of therapeutic approaches used to targeting each one of these key features for cancer development and progression (adapted from [16]).

Normal cells carefully control the production and release of growth-promoting signals, however, these signalling pathways are dysregulated in cancer cells [16]. The cancer cells can sustain the proliferation signalling, independently of the surrounding environment, by producing their own growth signals (*e.g.* platelet-derived growth factor) or overexpressing receptors involved in cell growth pathways [17]. Additionally, cancer cells are also capable of bypassing tumor suppressor genes that negatively regulate the cells' proliferation [16]. For example, the retinoblastoma protein (pRb), a key regulator of the cell cycle progression, is found inactivated in several cancer tissues [18]. Further, the p53 gene, whose protein is responsible for activating pro-apoptotic signals and coordinate the cell-cycle arrest in response to many cellular stresses and injuries, is mutated in 50% of tumor cases [15, 17]. Similarly, cancer cells can also promote the overexpression of anti-apoptotic proteins, such as B-cell lymphoma 2 (Bcl-2), further evading the programmed cell death [16]. Otherwise, the overexpression of telomerase, a deoxyribonucleic acid (DNA) polymerase that adds repeated segments to the DNA

telomers, sustains this limitless replicative potential of cancer cells [16, 19, 20]. Therefore, the telomerase expression in cancer cells maintains telomeres integrity during the successive replicative cycles, preventing DNA damage [16]. In healthy cells, excessive shortening of the telomeres can lead to the cells' senescence and/or apoptosis [19].

The capacity to stimulate the formation of new vessels is another important event in the cancer development, such will allow the influx of nutrients and oxygen as well as the elimination of metabolic wastes and carbon dioxide [21, 22]. For that purpose, the cancer cells can promote changes in the angiogenic machinery to favour the formation of new blood vessels [16, 23]. In this process, angiogenic inducers such as vascular endothelial growth factor-A (VEGF-A), angiopoietins, and platelet-derived growth factors are often overexpressed, whereas inhibitory molecules (*e.g.* thrombospondin-1 (TSP-1)) are downregulated [16]. The formation of new vessels can also influence the metastatic capacity of the tumors. The production of ECM-degrading enzymes and the loss of cell-cell and cell-ECM adhesion conjugated with the formation of new vessels will allow the colonization of different tissues by the tumor cells [23]. Furthermore, the tumor cells are highly capable to reprogram their metabolism accordingly the surrounding environment (*e.g.* Warburg effect) matching the high-energy demands for the continuous tumor growth, survival, proliferation, and long-term maintenance [16, 17]. Finally, the tumors can also take advantage of the immunologic system to support the tumor cells' growth, while avoiding the detection and consequent destruction [16]. For example, an inflammatory state in the tumor tissue will provide to the tumor microenvironment several bioactive molecules like growth factors, survival factors, proangiogenic factors, and extracellular matrix-modifying enzymes that are important for the cancer cells proliferation.

## 1.2. Conventional cancer therapies

The cancer treatment approaches often rely on chemotherapy, radiotherapy, surgery, immunotherapy, and hormone therapy or in the combination of thereof [24-28]. However, conventional therapeutic approaches present sub-optimal efficacy and can induce several side effects that can even lead to patient death. The removal of tumor tissue during the surgical procedure is impacted by the tumor location and often results in the incomplete removal of the cancer cells [29]. Therefore, patients are often subjected to a treatment modality involving the surgical removal of the tumor followed by sessions of chemotherapy and/or radiotherapy.

The chemotherapy has been the first-line treatment and aims to eradicate the cancer cells by using highly cytotoxic agents that can interfere in different cellular processes, such as

DNA synthesis (*e.g*. Daunorubicin and Mitoxantrone) and cellular division (Vincristine and Paclitaxel) [30-32]. Nevertheless, the direct administration of these highly cytotoxic agents in the bloodstream has some disadvantages that impair its effectiveness and discourage its application for long periods [5, 30]. The anticancer drugs often present a low water solubility, rapid degradation, short half-life in blood circulation, and poor bioavailability [30]. The low drug selectivity towards the cancer cells prompts the administration of higher drug doses to produce a therapeutic effect, which in turn intensifies the side effects.

Otherwise, the exposition of cancer cells to suboptimal concentrations of the highly cytotoxic agents also stimulates the development of drug resistance mechanisms [30]. The acquisition of multidrug resistance (MDR) phenotype by cancer cells allows them to bypass the action of anticancer drugs by the: i) continuous activation of DNA repair mechanisms; ii) increased efflux of drugs; iii) decreased influx of drugs; iv) mutations in the drug intracellular target; v) faster metabolism of the drugs; and vi) tight control over the cell death mechanisms [33-36]. For example, the cancer cells can overexpress efflux transporters such as P-glycoprotein (P-gp), a transmembrane protein that transport molecules to the exterior of the cell by the Adenosine Triphosphate (ATP) hydrolysis, avoiding the intracellular accumulation of the anticancer drugs and consequently circumvent its action [36]. Additionally, the DNA repair machinery is often upregulated in cancer cells, which counteracts the action of DNA targeting drugs, such as Daunorubicin [37]. Further, cancer cells also adapt the expression of the metabolic pathways and its constituents (*e.g*. cytochrome P450) to accelerate the degradation of the drugs reducing their concentration and consequently the therapeutic efficacy [38].

## 1.3. Drug combination as therapy

### 1.3.1. Drug combination

As previously described, the cancer cells can adapt in response to the exposition to chemotherapeutic drugs by activating different mechanisms that allow them to bypass the action of the drugs. In this field, the combinatorial therapies based on the simultaneous administration of multiple drugs emerged as a possible therapeutic approach to amplify the therapeutic efficacy of chemotherapy leading to the elimination of cancer cells [39]. This strategy explores the combination of cytotoxic drugs to achieve additive or synergistic effects [40]. The rationale underlying the development/testing of drug combinations has been to co-administer drugs that act on different targets increasing the elimination of cancer cells and reducing the effectiveness of the MDR mechanisms [41, 42]. Additionally, such improvement on the chemotherapy efficacy allows the reduction of the drug doses and thus minimizing the side-effects.

Currently, different drug combinations are used in the clinic to treat different cancers. O'Shaughnessy and colleagues reported that in phase III of clinical trial, the combination of Docetaxel and Capecitabine increased the time to disease progression from 4.2 to 6.1 months and the overall survival from 30 to 42%, when compared to the group treated only with Docetaxel [43]. Furthermore, Kosmas and colleagues also evaluated the application of a triple-drug combination, Paclitaxel-Ifosfamide-Cisplatin, in phase III of the clinical trial for the treatment of metastatic cervical cancer [44]. The results show that 62% of the patients respond to the combinatorial treatment and 26% present a complete response, *i.e.* the disappearance of all signs and symptoms of the disease for at least 1 month. Nevertheless, the authors also observed some haematologic toxicity. Similarly, Ding *et al.* evaluated the combination of three different drugs, Bortezomin, Camptothecin, and Doxorubicin (DOX) in the treatment of oral cancer [45]. The authors evaluated different drug ratios and determined that the combination 5-11-8 (a combination of Bortezomib at dose level 5 or 0.1 nmol/L; Camptothecin at a dose level of 11 or 400 nmol/L; DOX at a dose level of 8 or 6.25 nmol/L) presents an unique synergistic mechanism presenting high cytotoxicity in KB cancer cells, which was not observed in IMR90 control cells.

Despite the potential advantages of combining different drugs, this type of therapy is challenging due to the possible drug-drug and drug-bio interactions that can occur in the human body as well as to different biodistribution profiles, which will impact on the antitumoral efficacy of the drugs [35, 46]. Moreover, it is worth to notice that the combination of drugs can result in an antagonistic effect or only be effective (*i.e.* synergistic) for certain concentrations and combination ratios. Therefore, the development of new drug combinations allows the re-utilization and valorisation of chemotherapeutic drugs, but these combinations need to be extensively investigated.

### 1.3.2. Doxorubicin

DOX is an anthracycline drug widely used for the treatment of different types of cancer such as breast, lung, gastric, ovarian, thyroid, non-Hodgkin's and Hodgkin's lymphoma, and multiple myeloma [47, 48]. The DOX has a tetracyclic structure composed of 4 cyclohexane chains with daunosamine sugar, quinone-hydroquinone groups, carbonyl group, a methoxy substituent, and a primary alcohol group (Figure 2) [49].

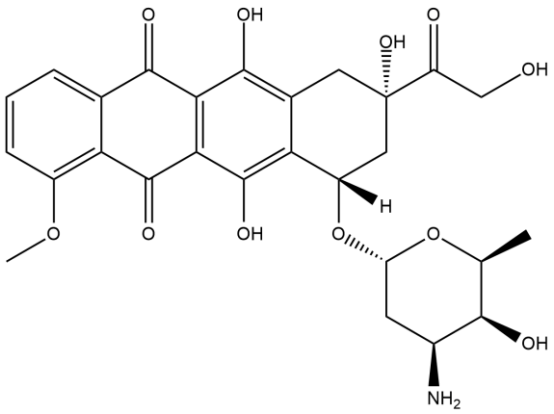


**Figure 2 -** Doxorubicin molecular structure.

The DOX anti-cancer mechanisms (Figure 3) were the subject of several basic research studies and clinical trials [48, 49]. The DOX intercalates between neighbouring DNA pairs through covalent and hydrogen bonds, which prevents the DNA replication and ultimately the protein synthesis [47]. Additionally, DOX also inhibits the topoisomerase II (Top II), an enzyme that can regulate the DNA condensation, relaxing the accumulated positive supercoils, as well as untangling the intertwined DNA strands [50]. During the DNA replication, the inhibition of Top II increases and stabilizes the cleavable enzyme-DNA complex and subsequently prevents the reconnection of the nucleotide strand after double-strand breakage [50, 51]. Such can lead to double-strand DNA breaks and inhibit DNA replication, leading to cell death by apoptosis [48, 50]. It is worth to notice that the Top II levels are higher in proliferating cells, so it increases the DOX selectivity to cancer cells [50]. Otherwise, the DOX can mediate the formation of reactive oxygen species that can induce the death of cancer cells. In this process, the DOX act as an electron acceptor in a reaction catalysed by cytochrome P450 reductase in the presence of NADH dehydrogenase producing DOX semiquinone radicals [48, 50, 51]. These semiquinone radical undergoes a transformation in C7 free radical, that can interact with molecular oxygen or other intracellular molecules such as lipids [51]. The semiquinone free radical causes oxidative damage that results in DNA damage or degradation. The interaction with oxygen molecules produces reactive free radicals like superoxide, hydroxyl radicals, and peroxides, which can cause DNA damages and lipids peroxidation [50]. However, the formation of reactive oxygen species (ROS) also contributes to the characteristic non-specific toxicity of DOX, namely the cardiac and cutaneous vascular side-effects [48, 52].

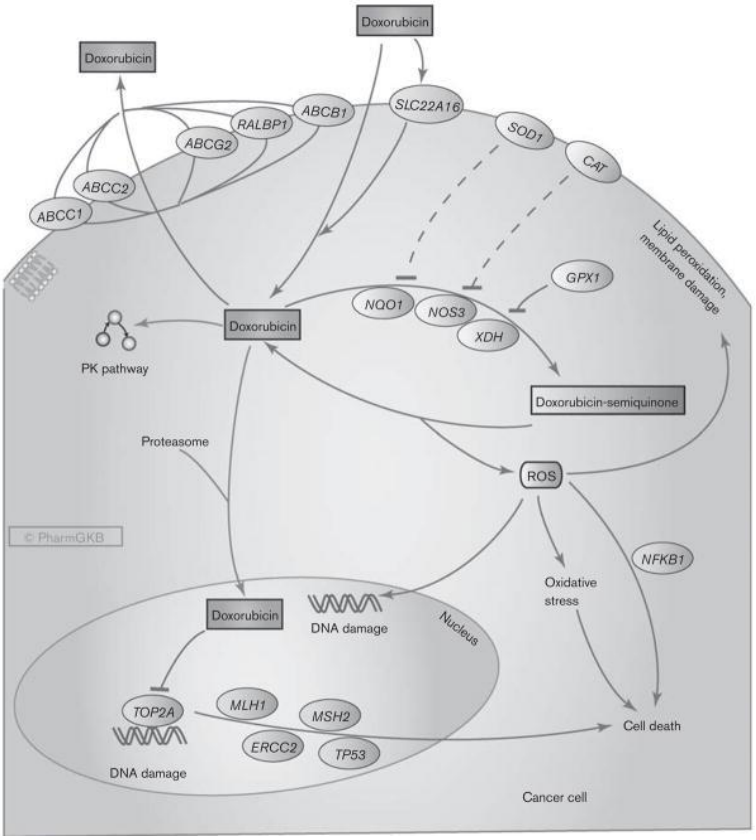


**Figure 3 -** Representation of the DOX interactions with intracellular components that can result in cell death (adapted from [47]).

### 1.3.3. Acridine Orange

Acridine Orange (AO) is a basic weak dye that was extracted for the first time from coal tar [53-55]. This compound can be used also as a pH indicator, photosensitizer, antitumoral drug, apoptosis detector, as well as antibacterial and antiparasitic agent [53, 54]. AO is a member of the class of aminoacridines that is acridine carrying two dimethylamino substituents at positions 3 and 6 (Figure 4). The AO has been used as a common fluorescent dye and recently it restarted to be explored as a possible anticancer drug for clinical applications [53]. Additionally, the AO derivates were already used in the clinic as antimicrobial and antimalarial agents [56]. The recent research focuses on the application of acridine-based molecules for cancer therapy aims to take advantage of the preferential accumulation of these molecules in acidic environments, such as the cancer tissue, through its intercalation within the double helix of DNA or by electrostatic attraction to the negatively charged phosphate groups (DNA and RNA) [54, 57-59]. Additionally, the AO low molecular weight facilitates the diffusion into the cytoplasm of the cells binding to DNA, ribonucleic acid (RNA), and acidic vesicles (*e.g.* lysosomes) [53, 54]. Despite the lack of information about the AO mechanism of action, a recent study indicates that the AO can act at the mitochondrial level being observed a reduction both

on the intracellular ATP content and expression of mitochondrial complex III in osteosarcoma cells treated with AO [60]. Additionally, the AO can also act as a photodynamic agent in response to irradiation with blue light [53]. Otherwise, the fluorescent properties of AO can be explored for the bioimaging of cancer cells, particularly in low pH conditions, AO emits orange light when excited by blue light, which has been used to identify apoptotic cells [56, 59].

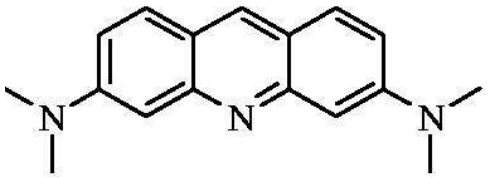

**Figure 4 -** Acridine Orange molecular structure (adapted from [59]).

However, the AO and the majority of the chemotherapeutic drugs present several issues that impact on the intravenous administration of these therapeutics, such as poor solubility, rapid metabolism, inconsistent bioavailability, and interaction with healthy tissues. Therefore, apart from identifying drug combinations with high therapeutic potential, it is also important to develop delivery systems that are capable of increasing the therapeutic selectivity and efficacy as well as reduce the systemic toxicity [55].

## 1.4. Nanotechnology in cancer therapy

In the past decades, the development of nanotechnology stimulated the production of drug delivery systems capable of improving cancer therapy [61]. The nano-sized transporters showed promising properties not only as drug or gene delivery systems (DDS) but also as biosensors, biomarkers, and imaging agents that can be applied in different areas [61-63]. Particularly, in cancer therapy, the application of nanomaterials as DDS can be very important to overtake the problems of conventional chemotherapy, such as the low water solubility of drugs, rapid degradation, and decreased bioavailability to obtain a great therapeutic result [64-66]. The nanomaterials' physicochemical properties confer to them the capacity to accumulate preferentially in tumor tissues, which increases the drug bioavailability, thus reducing the drug dose necessary to exert the therapeutic effect and avoid/decrease the therapeutics side effects. Further, the nanomaterials can also act as theragnostic agents combining the therapeutic (*e.g.* delivery of one or multiple drugs and/or photothermal agent), imaging (*e.g.* computed tomography), and diagnostic functions [61].

### 1.4.1. Nanoparticles properties

The utilization of nano-sized carriers has several benefits in comparison to traditional therapies such as increased drug solubility and stability, protection of drugs from premature degradation, metabolism and excretion, enhanced blood circulation time, and accumulation on the tumor tissues, which ultimately improves the therapeutic outcome [66-68]. Nevertheless, the nanomaterials must possess precise features that endow them with the capacity to be stable in the complex biological environment and achieve optimal therapeutic efficacy.

The nanoparticles' administration to the human body can be performed through oral, nasal, dermal, intramuscular, and intravenous routes [69, 70]. Among them, the intravenous injection is the most used administration method [70, 71]. Once in the bloodstream, the nanoparticles must avoid the rapid clearance (*i.e.* elimination in the urine) and recognition/accumulation by the reticuloendothelial system (RES), namely the liver and spleen [33, 72]. For this purpose, the nanomaterials should also minimize the adsorption of plasma proteins (*e.g.* serum albumin, complement compound, and immunoglobulins) to their surface, *i.e.* nanoparticles opsonization, since it will lead to the nanoparticles clearance by promoting their recognition by phagocytic cells [73-75]. The maintenance of the nanomaterials in the bloodstream increases their probability to extravasate into the tumor tissue, interact with the cancer cells, and release the therapeutic molecules [75]. These nanoparticles interactions with the human body are highly dependent on the size, charge, hydrophobicity, and chemical surface of the nanomaterials [73].

#### 1.4.1.1. Nanoparticles size

In the literature, it is often referred that the ideal nanoparticle size should be between 100 and 200 nm [76]. This size range takes into account the different barriers that the nanoparticles must face from the blood circulation until the interaction with the cancer cells. The nanoparticles' size should be superior to 5 nm to avoid the rapid clearance by renal filtration [61, 77]. Further, the size will also affect the nanoparticle retention in the spleen and liver. Nanoparticles should not have sizes lower than 50 nm since it allows them to extravasate and interacts with hepatocytes [61, 73, 75, 76]. Moreover, sizes superior to 200 nm are often associated with entrapment in the spleen [61, 78]. During blood circulation, particles with more than 750 nm are readily absorbed by monocytes, macrophages, and neutrophils through phagocytosis [61]. When the nanoparticles reach the tumor site, they must be able to extravasate from the blood vessels to the tumor tissue. Herein, it is worth to notice that due to the rapid proliferation of cancer cells, the tumors present an abnormal and leaky vasculature, fenestrae with 400 to 600 nm, and

an impaired lymphatic vasculature [61, 75]. Therefore, nanoparticles with sizes inferior to the tumor fenestrae will present a superior tumor accumulation and retention, a phenomenon defined as Enhanced Permeability and Retention (EPR) effect [75, 79]. Finally, the nanoparticles' size will also influence the penetration in the tumor tissue and cellular uptake [80]. Usually, larger nanoparticles accumulate in the peripherical regions of the tumors, whereas the smaller ones are more prone to penetrate into more interior regions [80, 81]. Otherwise, nanoparticles with 4 – 10 nm can transpose directly the cancer cells membrane into the cytoplasm, whereas bigger nanoparticles can be internalized through pinocytosis, a process that can be divided in clathrin-dependent endocytosis (≈20 nm, destined to lysosomes) or clathrin-independent endocytosis. The clathrin-independent endocytosis includes the macropinocytosis (size > 1 μm), clathrin- and caveolin-independent endocytosis (size ≈120 nm), and caveolin-dependent endocytosis (size ≈60 nm) [61, 79, 80].

#### 1.4.1.2. Nanoparticles charge

The nanoparticles' surface charge has also an important role in their blood circulation time and biodistribution. Nanoparticles with highly positive surface charges, values superior to + 10 mV, usually present an increased interaction with the proteins existent in the blood, which facilitates the opsonization and clearance [72]. Otherwise, negatively charged nanoparticles, values inferior to - 10 mV, are often associated with an increased RES uptake [72]. Moreover, the charge will also affect the interaction of the nanoparticles with the cells. Both normal and cancer cells present a higher uptake of positively charged nanoparticles [76]. Such occurs due to the interaction of the nanoparticles with the negatively charged components of the cell membrane [76]. Nevertheless, the membrane of tumor cells has a larger number of negatively charged components, such as phosphatidylserine or sialic acid, which further promote the uptake of positively charged nanoparticles [73]. Additionally, at the tumor site highly charged nanoparticles present a superior interaction with the components of the tumor extracellular matrix, hindering their penetration to deeper regions and tumor distribution.

Therefore, nanoparticles with a neutral surface charge (± 10 mV) can result in reduced absorption of proteins, increased blood circulation time, and more efficient tumor penetration, which makes this interval the most attractive for cancer treatment [72, 73, 75, 76].

#### 1.4.1.3. Nanoparticles shape

The shape of nanoparticles is an important property that can influence the blood circulation time, tumor uptake/cellular internalization, and the targeting in cancer drug

delivery [72, 76, 82]. For example, Blanco *et al.*, observed that spherical nanoparticles circulate in the central regions of the blood vessels, whereas discoidal particles have a dynamic that favour the interaction with the vessel walls, which can facilitate the extravasation to the tumor tissue [73]. Moreover, Decuzzi and colleagues compared the biodistribution and accumulation in the major organs of different silica structures like spheres, quasi-hemispherical, cylindrical, and discoidal nanoparticles [83]. These authors noticed that the discoidal nanoparticles had a superior performance with a decreased accumulation in the liver. Additionally, Arnida *et al.*, reported that gold-based nanospheres present a preferential accumulation in the liver, whereas the rod-like counterparts presented a higher blood circulation time and accumulation in tumors of female mice with 6 - 8 weeks old [84]. Otherwise, Ma and colleagues observed that spherical gold nanoparticles functionalized with poly(ethylene glycol) (PEG) have a higher cellular uptake that the particles with a nanospike and nanorod morphology [85].

#### 1.4.1.4. Surface composition of nanoparticles

The surface composition of nanoparticles is another important factor that influences their interaction with the human body [76]. The nanoparticles' surface modification with hydrophilic polymers such as PEG, poly(2-hydroxyethylmethacrylate) (PHEMA), and poly-2-ethyl-2-oxazoline (PEOZ) can increase their blood circulation time, reduce opsonization, and block the formation of the protein corona at the nanoparticle surface [61, 72, 73]. Moreover, the introduction of these surface modifications also improves the colloidal stability and biocompatibility of the nanoparticles [76]. Otherwise, targeting ligands (such as folic acid, Arginylglycylaspartic acid (RGD) sequences, and antibodies) can also be introduced in the nanoparticles' surface to improve their selectivity towards the cancer cells and reduce the nonspecific distribution [61, 68, 73, 86].

### 1.4.2. Nanoparticles for drug delivery

The nanoparticle application as DDS is the most explored strategy to overcome the disadvantages of conventional chemotherapy. These DDS protect the drugs from premature degradation, deliver high payloads to the cancer cells, and can be engineered to deliver the drugs in a spatial and temporally controlled manner. The reduced size of the nanoparticles confers to them the innate capacity to passively accumulate in the tumor tissue through the EPR effect [61]. Recent studies also revealed that apart from the EPR effect, in the tumor regions can occur vascular bursts that create transient openings and closings allowing the diffusion of the blood vessels' content to the tumor tissue [87]. Otherwise, targeting ligands can be immobilized in the nanoparticles' surface to specifically recognize a predetermined tumor marker [75]. These targeting agents (*e.g.* antibodies, peptides, and/or aptamers) are selected to explore ligand-receptor, antigen-

antibody, and other forms of molecular recognition with molecules that are overexpressed or uniquely expressed in tumor cells, such as the folate and transferrin receptors [33, 75].

Moreover, the nanoparticles can be engineered to release their cargo in response to specific stimuli, localized in the tumor region such as pH, redox environment, temperature, ATP, and enzymes; or with external origin like a magnetic field, near-infrared (NIR) light, and ultrasounds [61, 75]. For example, the high proliferation of cancer cells requires high levels of energy and uses the non-oxidative pathway, which leads to the production of lactate (Warburg Effect) and consequently the acidification of the tumor environment [33, 75, 88]. Therefore, the nanoparticles can explore the pH gradient, physiological pH ≈7.4 to tumor tissue pH ≈5.6, to trigger the release of chemotherapeutic drugs.

In this way, pH-responsive nanomaterials are usually composed of materials that change their conformation or suffer degradation in acid environments, such as chitosan, hyaluronic acid, calcium carbonate, or acid-labile chemical linkages [61, 88-91]. Other stimuli largely explored to control the drug release is the redox environment. In tumor tissues, the concentration of glutathione (GSH) is 100 to 1 000 times superior to that found in the extracellular fluids [61, 89]. The GSH/glutathione disulphide redox couple is the most important scavenger of ROS preventing damages in cancer cells. Therefore, this difference in the GSH concentration can be explored to degrade nanostructures composed of disulfide bonds (R-S-S-R) [61, 88, 89]. Furthermore, the nanoparticles can also be responsive to temperature changes [33, 88]. The unique organization of tumors combined with a defective vasculature and a high cellular proliferation renders to this tissue a temperature superior to the 37 ºC of the surrounding healthy tissues [61]. Therefore, temperature-responsive nanocarriers have been taking advantage of this temperature difference by using materials such as DNA, poly(2-(dimethylamino) ethyl methacrylate), and poly(N-isopropylacrylamide) [92-95]. Moreover, the differences between the extracellular concentration of ATP (0.4 mM) and that of the cell cytoplasm (10 mM) can also be explored to trigger the drug release when the nanoparticles reach the interior of the cell [61]. In these strategies, researchers take advantage of competitive binding interactions between ATP and the nanocarrier (*e.g.* coatings of ATP aptamers) to facilitate the drug diffusion from the nanoparticle to the external medium [96, 97]. Finally, it is also possible to develop nanoparticles responsive to enzymes (*e.g.* metalloproteases and esterases) that are overexpressed or exhibit increased activity in tumor tissue, using materials such as poly(β-amino ester) and PVGLIG polypeptide [33, 61, 98].

On the other side, magnetic fields, NIR light irradiation, and ultrasounds can be explored to prompt the drug release through the nanocarriers' thermal or mechanical degradation [89]. Magnetic-responsive nanoparticles produce heat in the presence of oscillating magnetic fields, which can then mediate the destruction or structural alterations in nanoparticles' structure [33]. Usually, nanomaterials responsive to the magnetic fields are composed of superparamagnetic iron oxide crystals [61, 89]. Similarly, the NIR laser irradiation (usually with a wavelength within the 700 to 950 nm) also explores the subsequent heat generation mediated by the nanomaterials to trigger the drug release. This strategy takes advantage of the inexistent or low interaction of the radiation in this region of the spectra with the biological components such as proteins, melanin, haemoglobin, collagen, and water, which confer a specific activation of the nanomaterials [61, 76]. The NIR responsive nanoparticles are commonly composed of gold, copper, carbon, or nanographene oxide, which are materials that presented a high absorption in the NIR region and effective light-to-heat conversion efficiencies [61, 76]. Lastly, the ultrasounds explore the sound waves to promote the vibration of the nanoparticles and consequent heat generation to trigger the drug release [33, 99, 100].

## 1.5. Gold core silica shell nanoparticles

During the last years, several different nanomaterials have been reported in the literature to act as a drug delivery system and/or imaging agent for cancer therapy. Considering the raw material used in DDS synthesis, the nanoparticles can be classified into two major classes: organic (*e.g.* lipid- and polymer-based nanomaterials) and inorganic nanoparticles (*e.g.* carbon, gold, graphene, iron, and silica nanoparticles) [6, 76, 101, 102]. Within the nanoparticles with theragnostic capacity, the gold core silica shell nanomaterials present promising properties that prompted its application in biomedicine, particularly in cancer therapy.

### 1.5.1. Properties of gold nanoparticles

The gold nanoparticles have increased relevance in biomedical applications due to their unique and desirable properties [86]. Gold is an inert and non-toxic metal that has resistance to oxidation and corrosion and is one of the less reactive known metals [86, 103]. This nobble metal has unique optical and electronic properties such as the surface plasmon resonance (SPR) phenomenon. The SPR is the collective oscillation of the electrons at the surface of gold nanomaterials in response to the irradiation with a light at a specific wavelength (*i.e.* resonance wavelength), which can result in the light scattering or absorption [104-106]. Additionally, the gold nanomaterials can be produced with different shapes (*e.g.* spheres, rods, cubes, stares, or others) each one

presenting specific optical and electronic properties that allow the fine-tuning of the SPR wavelength the NIR region. This shape control over the SPR wavelength has been increasingly explored to optimize the application of these nanomaterials in imaging and photothermal therapy [86, 105].

Nevertheless, the gold nanomaterials also present some limitations that hinder their direct application in the clinic [86, 105]. The gold nanoparticles easily interact with biological constituents due to the high capacity to create gold-sulfur bonds [86, 103, 107]. Particularly, as previously mentioned the adsorption of proteins will significantly impact the nano-bio interaction (*e.g.* clearance, RES recognition, nanoparticles uptake, and blood circulation time). Additionally, the gold nanoparticles application in imaging and therapy can include the exposition to high energy lasers pulses that can promote the nanoparticle reshaping and/or degradation due to the local temperature increase [105]. To address the limitations of gold nanoparticles, researchers have been exploring the combination of gold with other materials to reduce nonspecific adsorption of proteins and enhance the colloidal stability [108]. From the wide number of post-synthesis modifications of gold nanoparticles described in the literature (*e.g.* functionalization with PEG, polyoxazolines, dextran, chitosan, and liposomes), the introduction of a silica layer arises as one of the main coating alternatives for improving the antitumoral potential [107, 109-113].

### 1.5.2. Gold core silica shell nanoparticles

Gold nanoparticles produced with a mesoporous silica shell (AuMSS) have been widely explored due to their unique physical and chemical properties, being a promising solution to develop multifunctional anticancer nanomedicines (Figure 5). The mesoporous silica shell protects the gold core from degradation, provides a chemically inert and biocompatible surface, which improves the colloidal stability of gold nanoparticles, even in biological fluids or under high-energy radiation sources [114]. Besides gold core capacity to be applied in photothermal therapy (PTT) and bioimaging, the well-defined porous structure of silica can act as a reservoir for the loading of different pharmaceutical agents (*e.g.* drugs, genes, antibodies, and proteins), protecting them from premature degradation and avoiding their interaction with healthy tissues. This fact allows AuMSS nanoparticles application as drug delivery systems [88, 114]. Moreover, the silica shell does not compromise the photothermal efficacy of gold-based PTT agents since it is optically transparent to the NIR radiation (commonly used in PTT) [86]. Additionally, the silica shell possesses a high surface area that can be easily modified with different polymers and molecules, to avoid the immune system recognition, promote the tumor targeting, and confer a stimuli-responsive behaviour

(*e.g.* temperature, pH, enzymes, ROS) [86, 115-117]. Therefore, AuMSS can overcome the gold nanoparticles' limitations combining chemotherapy, bioimaging, and PTT. This multifunctional capacity improves AuMSS' therapeutic efficacy since different cancer pathways can be attacked, and synergetic interactions between the different therapies can occur [118].

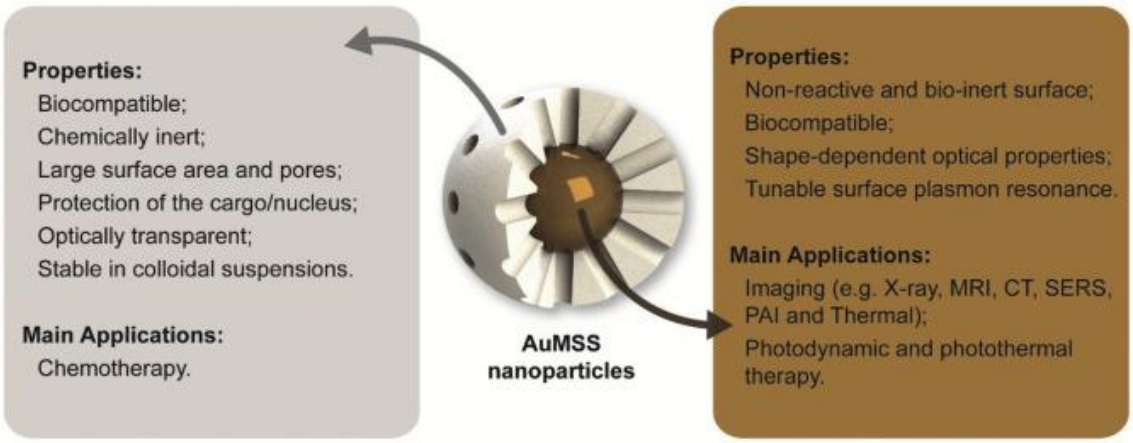


**Figure 5 -** Representation of AuMSS nanoparticles' main properties and applications (adapted from [86]).

In past years, different studies have been performed to produce the AuMSS nanoparticles in a controlled and reproducible way. The synthesis of AuMSS nanoformulations can be divided into two main steps: I) the production of the gold core with the desired size and shape; II) and the synthesis of a silica shell [86, 119]. Briefly, the synthesis of the gold core is accomplished by promoting the reduction of gold salts and subsequent nucleation of gold atoms in the presence of stabilizing agents (*e.g.* Hexadecyltrimethylammonium bromide - (CTAB)) that avoid the aggregation of gold cores. Afterward, the silica shell can be produced by using the conventional Stöber method or its derivations [111, 120]. During this procedure, a silica precursor (*e.g.* tetraethyl orthosilicate (TEOS)) is added to a basic solution of sodium hydroxide (NaOH) and start to condensate around de gold core by electrostatic interactions (the silanol molecules are negatively charged, whereas the stabilizing agents (*e.g.* CTAB) on the gold surface is positively charge) originating the silica shell. Moreover, the CTAB micelles that are added to the synthesis procedure act simultaneously as pore structuring agents, which leads to the formation of mesopores that constitute the AuMSS nanoparticles.

As gold nanoparticles, AuMSS can assume diverse shapes (*e.g.* rod, sphere, star, cage) since the gold cores can be produced thought different synthetic routes [86]. The spheres are the more stable shape and can be obtained under thermodynamically controlled

conditions. In contrast, the synthesis of non-spherical gold nanoparticles can be achieved by promoting an anisotropic growth (rods, cages, cages) of the gold core by using surfactants and structure-directing agents to block some of the growing directions [86, 104, 105]. The rod-shaped gold nanoparticles have been widely explored in cancer therapy applications and are produced through a seed-mediated growth methodology [121-124]. In this method, small spherical gold spheres (seeds) are added to a growing solution containing a gold salt (*e.g.* chloroauric acid), a reducing agent (*e.g.* ascorbic acid), high concentrations of CTAB, and a structure-directing agent (*e.g.* silver nitrate) to favour the longitudinal (rod-shaped) growth of the gold cores [104, 125]. Star-shaped gold nanoparticles are another anisotropic nanostructure produced from small gold cores using structure-directing agents such as poly(N-vinylpyrrolidone) that guide the nucleation of gold atoms originating the tips of gold nanostars [126]. Additionally, gold nanocages are usually produced through a galvanic replacement process, where silver nanocubes are gradually replaced by a gold precursor [105, 127]. Thus, the different gold shapes result in distinct optical and physicochemical properties, which can be fine-tuned to optimize the nanomaterials application in biomedical imaging (*e.g.* computerized tomography (CT), photoacoustic imaging (PA), surface-enhanced Raman spectroscopy (SERS), and thermal imaging) and therapy (*i.e.* PTT and Photodynamic therapy (PDT)) [86, 128-130]. As previously described, the mesoporous silica shell further increases the range of applications of gold nanomaterials by providing a superior particle stability and a higher capacity to encapsulate drugs (or other agents) [86, 131].

### 1.5.3. AuMSS nanoparticles biocompatibility

The application of nanoparticles in the biomedical field is closely linked to the nanoparticles' biosafety profile. Therefore, possible nano-bio interactions must be completely clarified (*e.g.* AuMSS biocompatibility, biodistribution, and pharmacokinetics) before they can be tested in clinical trials.

Dias *et al.* evaluated the biocompatibility of AuMSS nanospheres and nanorods in Human negroid cervix epithelioid carcinoma (HeLa) and Primary Normal Human Dermal Fibroblasts (FibH) cells. After 24, 48, and 72 h of incubation with different concentrations of nanoparticles (20 to 100 μg/mL) no toxicity was detected [118]. In another work, Reis *et al.*, developed AuMSS nanospheres coated with PEOZ and β-cyclodextrin (β-CD) [132]. The authors observed that non-coated AuMSS nanospheres at concentrations superior to 175 μg/mL reduced the cell viability to values inferior to 70%. However, the AuMSS functionalization with PEOZ and β-CD improved the nanoparticles cytocompatibility, being observed cell viabilities superior to 70% at concentrations of 200 μg/mL. Thakor *et al.* evaluated the biocompatibility and

biodistribution of 120 nm PEGylated AuMSS nanospheres after intravenous administration in mice [133]. The results demonstrated that the particles did not induce any significant damages or cytotoxic effects. However, 24 h after administration, the nanoparticles were mainly accumulated in the liver and spleen inducing a weak inflammatory response, which was normalized in 1 week. Otherwise, Luo *et al.* modified AuMSS nanospheres with β-CD, lactobionic acid, and PEG to deliver cisplatin to HepG2 tumor-bearing mice [134]. The results demonstrated that after 24 h of injection, 50 and 30% of nanoparticles were accumulated in the liver and spleen, respectively, with residual amounts detected in the heart, spleen, and kidney. Moreover, no damages or toxicity in vital organs were observed when high doses (1.15 mg/Kg) were administered.

### 1.5.4. AuMSS nanospheres

The AuMSS nanospheres are easily produced in a one-step easy to scale-up synthesis procedure, which combined with the unique physical and chemical properties make them appealing for applications in the clinic [118]. For example, the mass attenuation of the gold core, at energies superior to 80 kV, is higher than that of the iodinated contrast agents usually applied in the clinic, which can result in CT and Magnetic Resonance Imaging (MRI) images with superior resolution [135]. Wang and colleagues demonstrated that gold nanospheres can deliver gemcitabine to human pulmonary carcinoma cells and simultaneously act as CT contrast agents [136]. The CT imaging studies revealed that the gold nanoparticles' brightness was higher than that of Ultravist (iodine-based contrast agent). Further, the CT value of the gold nanoparticles was almost 2-times superior to that of Ultravist, at gold or iodine concentrations of 25 mM. In another study, Kobayashi and co-workers developed AuMSS nanospheres with 136 nm (gold core of 17 nm) to be applied as a contrast agent in CT [137]. The nanoparticles produced exhibited an attenuation capacity almost seven times higher than Iopamiron®, a commercial iodine-based X-ray contrast agent. Moreover, the authors also described that 5 min after the particles are injected, the liver and spleen contrast increased (76.7 and 96.5 Hounsfield units (HU) to 115.0 and 120.2 HU, respectively) and remained constant for 2 days.

Contrary to what is observed with the other morphologies, the lack of absorption in the NIR region of the spectra impairs the application of AuMSS nanospheres in cancer photothermal therapy since these nanoparticles only present an absorbance band in the visible region (500 - 550 nm) of the electromagnetic spectrum [105, 118, 138]. However, the pores of the silica shell enable the encapsulation of high payloads of therapeutic agents. Therefore, the application of spherical AuMSS in therapy has been principally focused on drug delivery [86, 119, 132]. Dias and colleagues reported the loading of DOX

on AuMSS nanospheres and its delivery to HeLa cancer cells [118]. The application of DOX loaded AuMSS nanoparticles in 2D and 3D cell culture models revealed the successful internalization in HeLa cells and penetration in 3D models of HeLa spheroids. Moreover, the authors observed that after 48 h of incubation with HeLa cells, the DOX loaded AuMSS nanoparticles at 100 μg/mL mediate the reduction of the HeLa cells viability to ≈20% [118]. Similarly, Ramasamy applied cinnamaldehyde loaded AuMSS nanoparticles in the treatment of bacteria [139]. The obtained results demonstrated that the cinnamaldehyde encapsulation in AuMSS nanospheres potentiated the antimicrobial activity, which inhibited the biofilm formation by *Escherichia coli*, *Pseudomonas aeruginosa*, *methicillin-sensitive Staphylococcus aureus*, and *methicillin-resistant Staphylococcus aureus*

Despite the high potential of AuMSS nanospheres for bioimaging and drug delivery applications, their clinical translation is hindered by their reduced circulation time in the bloodstream and specificity for the tumoral tissue. Therefore, researchers have been focusing on the development of novel AuMSS coatings capable of improving the nanoparticles circulation time and control over the drug release. Simultaneously, the study and development of combinatorial therapies based on the co-administrations of multiple drugs have been explored to increase the therapeutic efficacy of chemotherapy, reducing the effectiveness of the MDR mechanisms. These characteristics will improve the accumulation of nanoparticles within the tumor tissue, while simultaneously decrease the chemotherapeutics interactions with healthy tissues, which ultimately enhances the therapeutic effect.

## Aims

The main goal of this dissertation was to design a dual drug combination (DOX and AO) to be encapsulated in AuMSS nanospheres (Figure 6). Moreover, a novel AuMSS surface modification based on 3-(Triethoxysilyl)propyl isocyanate-Poly(ethylene glycol)-4-Methoxybenzamide (TPANIS) was developed to improve nanoparticles' blood circulation time as well as increase AuMSS specificity to cancer cells.

The specific aims of this dissertation are:

- Evaluation of the DOX/AO combinatorial potency;
- Synthesis of TPANIS polymer;
- Synthesis, functionalization, and loading of the AuMSS nanospheres;
- Characterization of the AuMSS' physicochemical properties;
- Characterization of nanoparticles' cellular uptake;
- Evaluation of the cytotoxic activity of the DOX and AO loaded AuMSS nanoformulations.

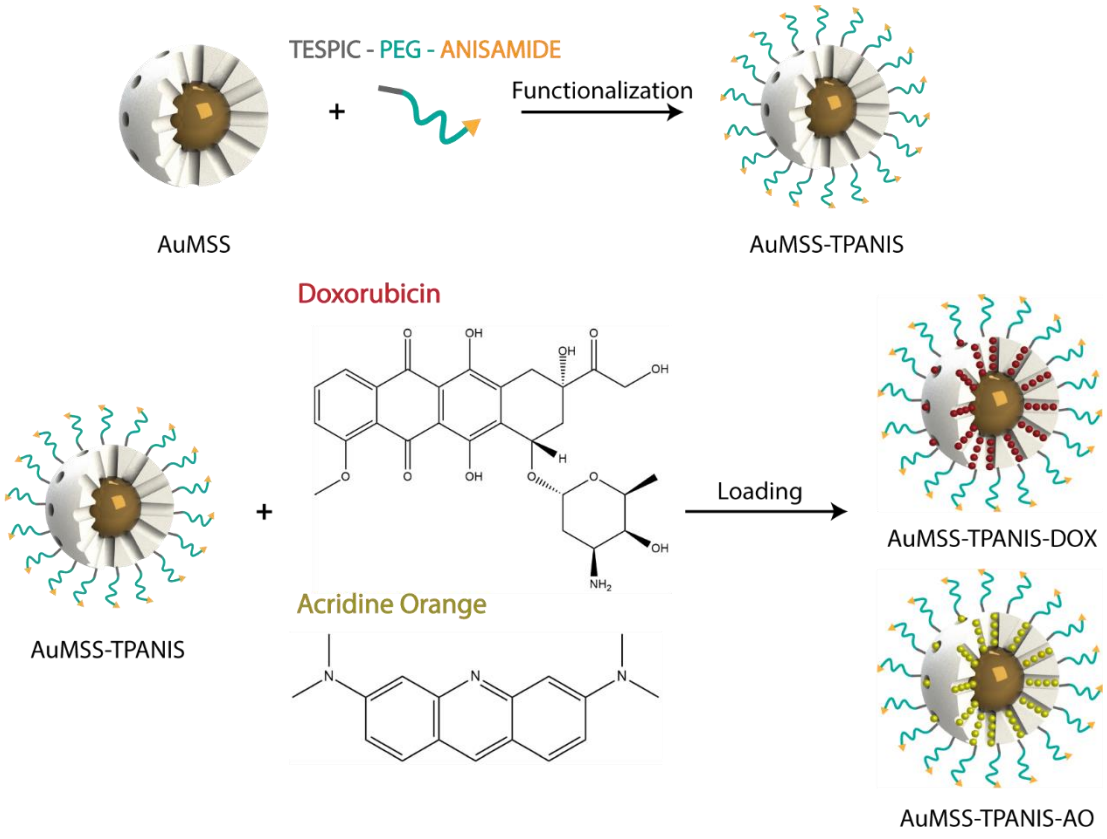


**Figure 6 -** Scheme of the nanoparticles' modification with the TPANIS polymer and encapsulation of DOX and AO.

# Chapter 2

# Experimental Section

# 2. Experimental Section

## 2.1. Materials

Hydrogen tetrachloroaurate (III) hydrate ($HAuCl_4$) was purchased from Alfa Aesar (Karlsruhe, Germany). Tetraethyl orthosilicate (TEOS) and tetrahydrofuran (THF) were obtained from Acros Organics (Geel, Belgium). Hexadecyltrimethylammonium bromide (CTAB) was bought from Tokyo Chemical Industry Europe (Zwijndrecht, Belgium). Hydrochloric acid (HCl) was acquired from Panreac (Barcelona, Spain). Methanol (MetOH) was obtained from VWR International (Carnaxide, Portugal). Dulbecco's Modified Eagle medium-high glucose (DMEM-HG), Dulbecco's Modified Eagle Medium: Nutrient Mixture F-12 (DMEM-F12) resazurin, ethanol (EtOH), formaldehyde, trypsin, Acridine Orange (AO), fluorescein isothiocyanate (FITC), Phosphate-buffered saline (PBS) solution and 3-(Triethoxysilyl)propyl isocyanate (TESPIC), Poly(ethylene glycol) (PEG) Mw: 10 000 g/mol), Dichloromethane (DCM), 4-Methoxybenzamide or Anisamide (ANIS) (Mw: 151.16 g/mol) were purchased from Sigma–Aldrich (Sintra, Portugal). Fetal bovine serum (FBS) was acquired to Biochrom AG (Berlin, Germany). Primary Normal Human Dermal Fibroblasts (FibH) cells were acquired from PromoCell (Labclinics, S.A., Barcelona, Spain). Human negroid cervix epithelioid carcinoma (HeLa) cells (ATCCs CCL-2t) and Michigan Cancer Foundation-7 (MCF-7) cells were purchased from ATCC (Middlesex, UK). Doxorubicin hydrochloride (DOX) was obtained from Carbosynth (Berkshire, UK). Hoechst 33342® and wheat germ agglutinin conjugate Alexa 594® WGA-Alexa Fluor® 594) were bought from Invitrogen (Carlsbad, CA). Cell culture t-flasks were obtained from Orange Scientific (Braine-l'Alleud, Belgium). Cell imaging plates were acquired from Ibidi GmbH (Munich, Germany).

## 2.2. Methods

### 2.2.1. Cytotoxic activity of DOX and AO in cell culture

The cytotoxicity profile of DOX and AO in HeLa and MCF-7 cells was evaluated through a resazurin-based assay [140]. In this method, viable cells mediate the reduction of resazurin (a non-toxic reagent) to a red fluorescent compound – resorufin [141]. Briefly, HeLa or MCF-7 cells were seeded in 96-well culture plates with the respective culture medium (DMEM-HG or DMEM-F12) at a density of 10 000 cells/well, and cultured for 24 h, at 37 ºC and 5% $CO_2$. Afterward, the cells were incubated with increasing drug concentrations for 48 h. Then, the medium was removed, and cells were incubated with 10% (v/v) of resazurin (1 mg/mL), at 37 °C and 5% $CO_2$, during 4 h. The produced resorufin, present in the culture medium, was then quantified by using a microwell plate reader (Spectramax Gemini XS, Molecular Devices LLC, USA) at an excitation/emission

wavelength of λex = 560 nm and λem = 590 nm. Cells incubated with EtOH were used as a positive control ($K^+$), whereas cells without being exposed to DOX and AO were used as a negative control ($K^-$). Posteriorly, the drugs' dose-response curves were traced to determine the DOX and AO inhibitory concentrations (ICs), IC20, IC50, and IC80, using OriginLab software (trial version, OriginPro, OriginLab Corporation, MA, USA) [142].

### 2.2.2. Screening of DOX:AO combinations

After calculating the ICs of DOX and AO, different DOX and AO combination ratios (DOX:AO) were tested in HeLa and MCF-7 cell lines. For that purpose, cells were seeded in 96-well culture plates with the respective culture medium (DMEM-HG or DMEM-F12) at a density of 10 000 cells/well, and cultured for 24 h, at 37 ºC and 5% $CO_2$. After this period, different drug ratios were incubated for 48 h. The overall tested drug concentration was related to the IC20, IC50, and IC80 calculated for DOX and was selected in order to be possible to compare the effect of DOX:AO combinations with the single administration of DOX (Table 1).

**Table 1** - DOX and AO molar concentrations used in each DOX:AO ratios tested in HeLa cancer cells.

| Ratio DOX:AO | 0.824 μM (IC20) | | 1.589 μM (IC50) | | 3.063 μM (IC80) | |
|---|---|---|---|---|---|---|
| | DOX (μM) | AO (μM) | DOX (μM) | AO (μM) | DOX (μM) | AO (μM) |
| **5:1** | 0.69 | 0.14 | 1.32 | 0.26 | 2.55 | 0.51 |
| **4:1** | 0.66 | 0.16 | 1.27 | 0.32 | 2.45 | 0.61 |
| **3:1** | 0.62 | 0.21 | 1.19 | 0.40 | 2.30 | 0.77 |
| **2:1** | 0.55 | 0.27 | 1.06 | 0.53 | 2.04 | 1.02 |
| **1:1** | 0.41 | 0.41 | 0.79 | 0.79 | 1.53 | 1.53 |
| **1:2** | 0.27 | 0.55 | 0.53 | 1.06 | 1.02 | 2.04 |
| **1:3** | 0.21 | 0.62 | 0.40 | 1.19 | 0.77 | 2.30 |
| **1:4** | 0.16 | 0.66 | 0.32 | 1.27 | 0.61 | 2.45 |
| **1:5** | 0.14 | 0.69 | 0.26 | 1.32 | 0.51 | 2.55 |

Subsequently, the 3 most promising drug ratios were selected and the dose-response curves and IC20, IC50, and IC80 values were determined for each drug ratio (please see section 2.2.1.). Additionally, the Combination Index (CI) was calculated according to the Chou–Talalay method [143, 144]. The CI value for the dual combinations was calculated according to the following equation (1):

$$\text{Combination Index} = \frac{\text{IC50 (Doxorubicin+Acridine Orange)}}{\text{IC50 Doxorubicin}} \quad (1)$$

Combination index values were associated with different effects of the drugs in cancer cells (CI < 0.8, synergistic); (0.8 < CI < 1.2, additive) and (CI > 1.2, antagonistic).

### 2.2.3. Synthesis of AuMSS nanospheres

AuMSS nanospheres were synthesized through a method previously described in the literature [132]. Initially, a solution of 0.05 g of CTAB and 0.6 mL of NaOH (0.5 M) were added to 24 mL of ultrapure water under stirring at 80 ºC. Then, 1 mL of formaldehyde (3.7%) and 0.8 mL of $HAuCl_4$ (0.05 M) were added to the previous solution to obtain the gold nanospheres. After 10 min, 910 μL of TEOS (33% v/v in MetOH) were added and the resulting solution reacted for 1 h under reflux and stirring conditions. The AuMSS nanospheres were recovered by centrifugation at 11 000g and 25 ºC.

### 2.2.4. Removal of the surfactant template

The highly cytotoxic CTAB surfactant template was removed from nanoparticles by adapting a solvent-based approach described in the literature [118]. Briefly, AuMSS nanospheres were resuspended in an acidic solution (HCl 10% v/v in EtOH), sonicated, and centrifugated (18 000g for 20 min at 25 ºC). After several washing steps in the acid solution, nanoparticles were washed two times with EtOH (100% v/v) and ultrapure water to allow the complete elimination of the CTAB and HCl residues. Finally, nanoparticles were recovered by centrifugation (18 000g for 20 min at 25 ºC) and freeze-dried.

### 2.2.5. Synthesis of TESPIC-PEG-ANIS

First, the reaction of PEG and ANIS was performed by adapting an approach described in the literature [145]. PEG (0.5 mmol) was dissolved in 3 mL of dry DCM under a nitrogen atmosphere and magnetic stirring. Then, PEG was activated with 1,1′-Carbonyldiimidazole (CDI) (89.1 mg) that was added dropwise to the previous solution and left under a nitrogen atmosphere and vigorous stirring for 6 h. After that, ANIS (151.6 mg) was dissolved in 6 mL of EtOH (100% v/v) and added to the activated PEG and left under stirring for 14 h. Afterward, the excess of DCM was removed by evaporation (Rotavap®R-215, Büchi, Switzerland) and the obtained PEG-ANIS (PANIS) was hydrated with ultrapure water, sonicated, and freeze-dried.

Subsequently, PANIS polymer was modified with TESPIC, to allow their chemical coupling to the surface of AuMSS nanospheres, through a method previously described by Moreira and co-workers [140]. For that purpose, PANIS (200 mg) was dissolved in

60 mL of THF anhydrous under a nitrogen atmosphere and magnetic stirring, at 60 ºC for 6 h. Then, 100 µL of TESPIC were added to the mixture and left to react for 24 h. The PANIS silane derivative (TPANIS) was recovered by evaporation (Rotavap®R-215, Büchi, Switzerland). After that, the TPANIS polymer was purified by dialysis in ultrapure water and then recovered by freeze-drying.

The successful synthesis of TPANIS was confirmed by using the Transform Infrared Spectroscopy (FTIR) analysis using a Nicolet iS10 spectrometer (Thermo Scientific Inc., MA, USA).

### 2.2.6. AuMSS functionalization

The TPANIS was chemically linked to the AuMSS surface by using a post-synthesis grafting methodology as previously described in the literature [132]. First, 10 mg of AuMSS nanospheres were resuspended in 10 mL of EtOH (33% v/v, at pH 4) and sonicated for 5 min. Then, 30 mg of TPANIS were dissolved in 30 mL of EtOH (33% v/v, at pH 4) and were added to the nanoparticles' solution (AuMSS/TPANIS ratio of 1:3 w/w) and stirred for 24 h (Figure 7). After this period, AuMSS-TPANIS nanoparticles were washed several times in ultrapure water and recovered by centrifugation (6 000 g for 25 min at 25 ºC).

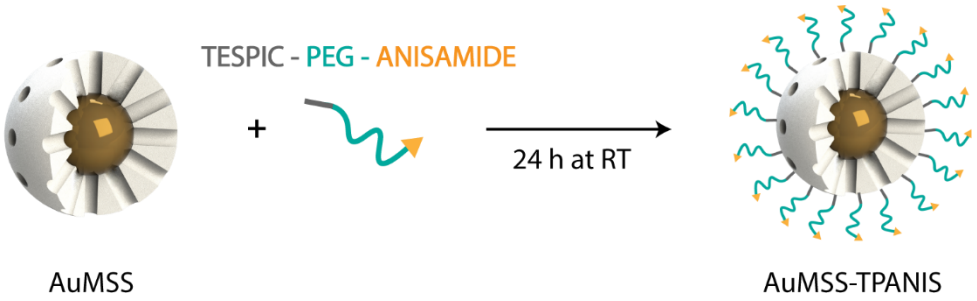


**Figure 7** - Representation of the nanoparticles' functionalization with TPANIS, RT -room temperature.

### 2.2.7. Characterization of the AuMSS nanoformulations' physicochemical properties

#### 2.2.7.1. Morphological characterization and size analysis

The morphology of AuMSS and AuMSS-TPANIS nanospheres was characterized by Transmission Electron Microscopy (TEM - Hitachi-HT7700, Japan). For that purpose, the nanoparticles were placed on formvar-coated copper grids and dried at room temperature. The TEM images were acquired at an accelerating voltage of 80 kV or 200 kV with different magnifications. After that, the silica shell thickness and gold core size were measured by using specific software (Image J 2.0.0, NIH Image, USA).

The size distribution of AuMSS and AuMSS-TPANIS was determined by Dynamic Light Scattering (DLS) using a ZetaSizer NanoZS (Malvern Instruments Ltd., Worcestershire, United Kingdom (UK)). Furthermore, preliminary stability assays were performed by assessing the variation in the size distribution of AuMSS nanoformulations dispersed in ultrapure water for 24 h.

#### 2.2.7.2. Zeta potential analysis

The AuMSS and AuMSS-TPANIS nanospheres surface charge was measured by using the Zetasizer Nano ZS equipment (Malvern Instruments, Worcestershire, UK). The zeta potential data were collected at 25 °C in a disposable capillary cell in ultrapure water.

#### 2.2.7.3. Fourier transform infrared spectroscopy analysis

The FTIR spectroscopy was used to evaluate the success of the AuMSS purification and functionalization with the TPANIS polymer. Thus, the FTIR spectra of AuMSS and AuMSS-TPANIS were acquired in a Nicolet iS10 spectrometer (Thermo Scientific Inc., Massachusetts, USA) with a spectral resolution of 4 $cm^{-1}$ ranging from 4 000 $cm^{-1}$ to 600 $cm^{-1}$. Moreover, in all the acquired data a baseline correction and atmospheric suppression were performed to avoid any possible interferences. Data analysis was executed in the OMNIC spectra software (Thermo Scientific).

#### 2.2.7.4. Thermogravimetric analysis

The TPANIS content on the AuMSS nanospheres was measured by performing the Thermogravimetric analysis (TGA) of the nanoformulations. For that purpose, the AuMSS and AuMSS-TPANIS were heated up to 600 ºC, at a heating rate of 10 ºC/min, under an inert atmosphere on an SDT Q600 equipment (TA Instruments, USA) and the weight losses were recorded along time.

### 2.2.8. Drug loading

The DOX and AO loading in AuMSS and AuMSS-TPANIS nanospheres was accomplished through a method previously described in the literature [140]. Nanoformulations were resuspended in 10 mL of MetOH containing DOX or AO (200 ug/mL), sonicated for 15 min, and stirred under magnetic agitation for 48 h at room temperature. Afterward, the drug-loaded nanoparticles were recovered by centrifugation (18 000g for 20 min at 4 ºC) and freeze-dried. The supernatant was used to quantify the AO and DOX loading content.

The loading quantification was performed by determining the supernatant absorbance at 485 nm for DOX and 489 nm for AO, using a Ultraviolet-visible (UV-vis) Spectrophotometer (Thermo Scientific Evolution™ 201 Bio UV-Vis Spectrophotometer,

Thermo Fisher Scientific Inc., USA). The DOX concentration was calculated using a calibration curve (Abs=0.0162C-0.001; $R^2$=0.999), whereas AO concentration was calculated using a calibration curve (Abs=0.1981C–0.0033; $R^2$=0.999). The encapsulation efficiency (E.E) was calculated using the equation (2):

$$\text{E. E (\%)} = \frac{\text{(Initial drug weight-Drug weight in the supernatant)}}{\text{Initial drug weight}} \times 100 \qquad (2)$$

### 2.2.9. Evaluation of AuMSS nanoparticles' cytocompatibility

The cell viability of cancer cells (HeLa and MCF-7) and normal cells (FibH), when incubated with AuMSS and AuMSS-TPANIS, were evaluated by a resazurin-based assay [145]. Briefly, cells were seeded into 96-well flat-bottom culture plates with the respective culture medium (DMEM-F12 or DMEM-HG), at a density of 10 000 cells/well and cultured at 37 °C in an incubator with a humidified atmosphere containing 5% $CO_2$. Then, cells were incubated with different concentrations of AuMSS, ranging from 25 to 200 μg/mL for 24, 48, and 72 h of incubation. At each time point, the medium was replaced, and cells were incubated with a solution of resazurin (10% v/v), at 37 °C and 5% $CO_2$, during 4 h. After that, the resazurin assay was performed to determine the cancer cells' viability, using the method described above. Cells incubated with EtOH (99.9%) and cells only incubated with culture medium were used as positive ($K^+$) and negative ($K^-$) controls, respectively.

### 2.2.10. Evaluation of nanoparticles' cellular uptake

The uptake of AuMSS and AuMSS-TPANIS nanoparticles by FibH, HeLa, and MCF-7 cells was determined by fluorescence spectroscopy, through a method described by Reis and colleagues [132]. Briefly, cells were seeded at a density of 10 000 cells/well in 96-well flat-bottom culture plates and cultured for 24 h at 37 °C and 5% $CO_2$. Then, cells were incubated with the FTIC-labelled AuMSS and AuMSS-TPANIS nanoparticles at 200 μg/mL for 4 h. One of the test groups was previously treated with free ANIS (10 μg/mL) for 3 h. Afterward, the cells were washed with ice-cold Krebs Ringer Buffer (KRB) to remove the non-internalized particles and lysed with 1% Triton X-100 in KRB for 30 min at 37 °C. The FITC fluorescence was quantified with a spectrofluorometer (Spectramax Gemini XS, Molecular Devices LLC, USA) at an excitation/emission wavelength of λex = 480 nm and λem = 570 nm. Cells only incubated with KRB were used as a negative control.

### 2.2.11. Characterization of 2D cell cytotoxicity profile AuMSS-TPANIS

The cytotoxic effect of the AO or DOX-loaded AuMSS-TPANIS nanoparticles was evaluated on HeLa and MCF-7 cells, through the resazurin assay. Briefly, cells were seeded in a 96-well plate at a density of 10 000 cells/well and cultured for 24 h at 37 °C and 5% $CO_2$. After 24 h, cells were incubated with DOX loaded AuMSS-TPANIS and AO loaded AuMSS nanoparticles (with DOX/AO ratios of 2:1, 1:1, and 1:2) for 48 h. Afterward, the viability of HeLa and MCF-7 cells was measured by using the resazurin assay as previously described. Cells incubated with EtOH (99.9%) and cells only incubated with culture medium were used as positive ($K^+$) and negative ($K^-$) controls, respectively.

### 2.2.12. Statistical analysis

All data are presented as the mean ± standard deviation (s.d.). The statistical analysis was performed using One-way ANOVA test. A value of p lower than 0.05 ($p < 0.05$) was considered statistically significant. The Statistical analysis was performed using GraphPad Prism v.7.0 software (GraphPad Software, USA).

# Chapter 3

# Results and Discussion

# 3. Results and Discussion

## 3.1. Cytotoxic activity of DOX and AO

In order to evaluate the effect of the DOX:AO combination towards cancer cells, an initial screening of the DOX and AO therapeutic capacity was first performed in HeLa cancer cells followed by the testing of the drug with lowest IC50 in MCF-7 cancer cells (Figure 8). With that in mind, the cancer cells were incubated 48 h with crescent drug concentrations and the cancer cells' viability was determined. The obtained results were used to calculate the dose-effect curves and IC values (*i.e.* IC20, IC50, IC80). In Figure 8 B and C, it is possible to observe that the DOX display a higher cytotoxic effect in HeLa cells than AO. In fact, the IC50 of DOX was about 6.8-times lower than that of AO (IC50 (DOX) = 1.59 μM; IC50 (AO) = 10.85 μM).

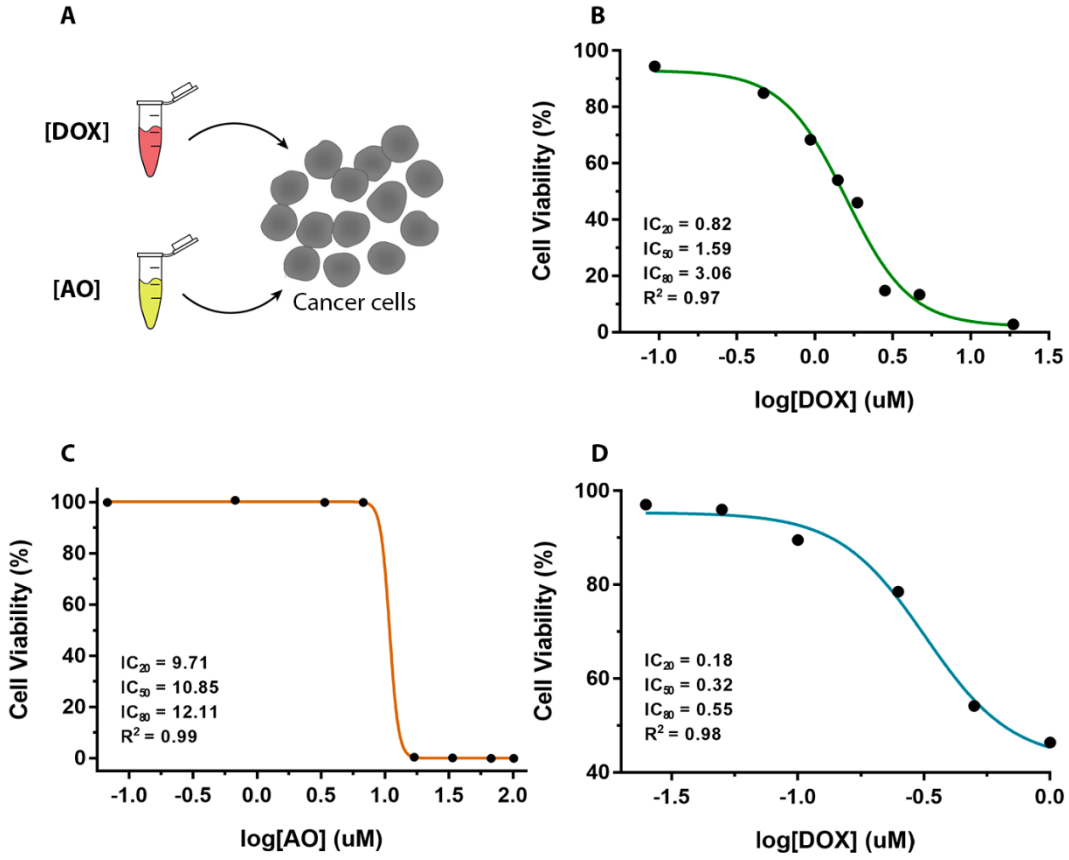


**Figure 8 -** Evaluation of the DOX and AO therapeutic capacity in HeLa and MCF-7 cancer cells. (A) Schematics of the cancer cells' treatment with DOX and AO in cancer cells. Dose-response curves of DOX (B) and AO (C) to HeLa Cells. Dose-response curves of DOX (D) to MCF-7 and respective ICs.

Considering the DOX superior anticancer capacity in HeLa cancer cells, the MCF-7 cancer cells dose-response curve to DOX and correspondent IC values were also determined. The obtained data demonstrated that the DOX produced a greater cytotoxic

effect in MCF-7 cancer cells, presenting an IC50 of 0.32 μM, which is 5-times lower than that obtained in HeLa cancer cells (Figure 8 D).

## 3.2. Evaluation of drugs combination

After determining the DOX and AO ICs values in HeLa and MCF-7 cancer cells, a preliminary screening of the DOX:AO therapeutic efficacy was assessed with HeLa cells (Figure 9). For that purpose, HeLa cancer cells were incubated with different DOX:AO ratios (5:1 to 1:5) at a total drug concentration of 0.62, 1.59, and 3.06 μM, which correspond to the IC20, IC50, and IC80 of DOX. Further, to compare the effect of the DOX:AO drug combination, the HeLa cancer cells' response to equivalent DOX concentrations (monotherapy) was also studied. The obtained results show that a superior cytotoxic effect can be obtained with the DOX:AO drug combination when compared to the single DOX administration, principally at concentrations superior to the IC20 (0.62 μM). Moreover, considering the three tested concentrations in general, the DOX:AO drug ratios of 2:1, 1:1, and 1:2 display the most effective anticancer effect against the HeLa cancer cells, presenting the lowest cell viability from the tested groups. These results show the advantage of the DOX:AO drug combination, allowing the application of lower doses of DOX, which can decrease both the therapy cost and the side effects (*e.g.* cardiotoxicity, hepatotoxicity, and nephrotoxicity) [47, 146].

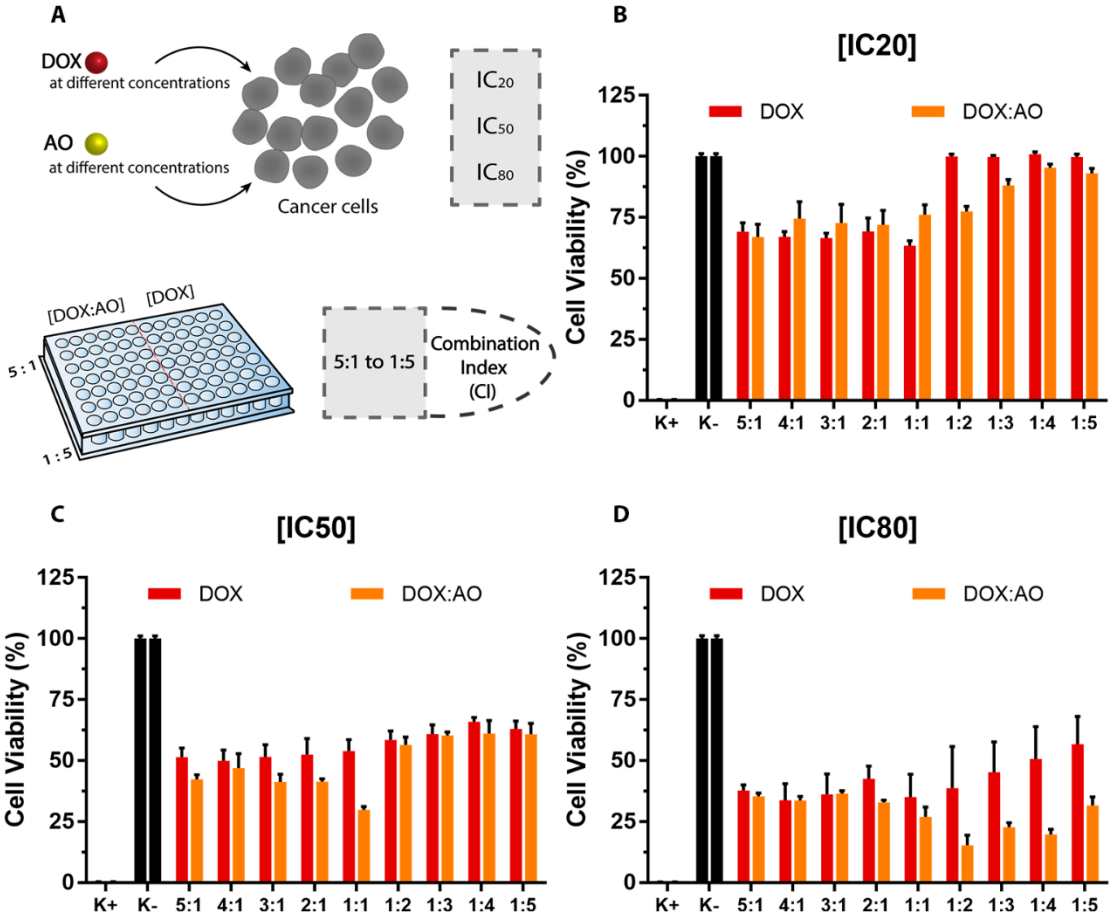


**Figure 9 -** Evaluation of the therapeutic efficacy of DOX:AO drug ratios in HeLa cells. (A) Schematics of the DOX and AO combination and evaluation in cancer cells. (B-D) HeLa cell viability after the administration of DOX or DOX:AO drug ratios (5:1 to 1:5) at a total drug concentration of 0.62, 1.59, and 3.06 μM. Data are presented as mean ± s.d., n = 5.

Afterward, the HeLa and MCF-7 cells dose-response curves were traced to determine the IC20, IC50, and IC80 of 2:1, 1:1, and 1:2 DOX:AO drug ratios (Figure 10). As expected, the IC values of the DOX:AO drug combinations were lower than those obtained for the single DOX administration in both cell lines. For example, the IC50 for 2:1, 1:1, and 1:2 DOX:AO drug ratios in HeLa cancer cells was 0.829, 0.741, and 0.937 μM, respectively, whereas the value obtained for single DOX was 1.59 μM. Moreover, to further evaluate the therapeutic potential of DOX:AO combinations, the combination index was calculated for 2:1, 1:1, and 1:2 DOX:AO drug ratios (Figure 11). The results obtained for HeLa cells revealed that these DOX:AO combinations induce a synergistic effect (CI values between 0.4 and 0.75), except the 1:2 ratio at a drug concentration equivalent to IC80. Otherwise, the 2:1 DOX:AO drug ratio presented an antagonistic effect in MCF-7 cells, whereas the 1:1 and 1:2 DOX:AO drug ratio presented a synergistic effect (CI values between 0.25 and 0.75) at concentrations equivalent to IC20 and IC50. These results

indicate that the DOX:AO combination has a superior performance in HeLa cells. Nevertheless, in a therapeutic point-of-view, the DOX:AO drug combination can be tailored to present synergistic cytotoxic effects in both cancer cell lines, reducing the drug dose necessary to eradicate the tumor [41].

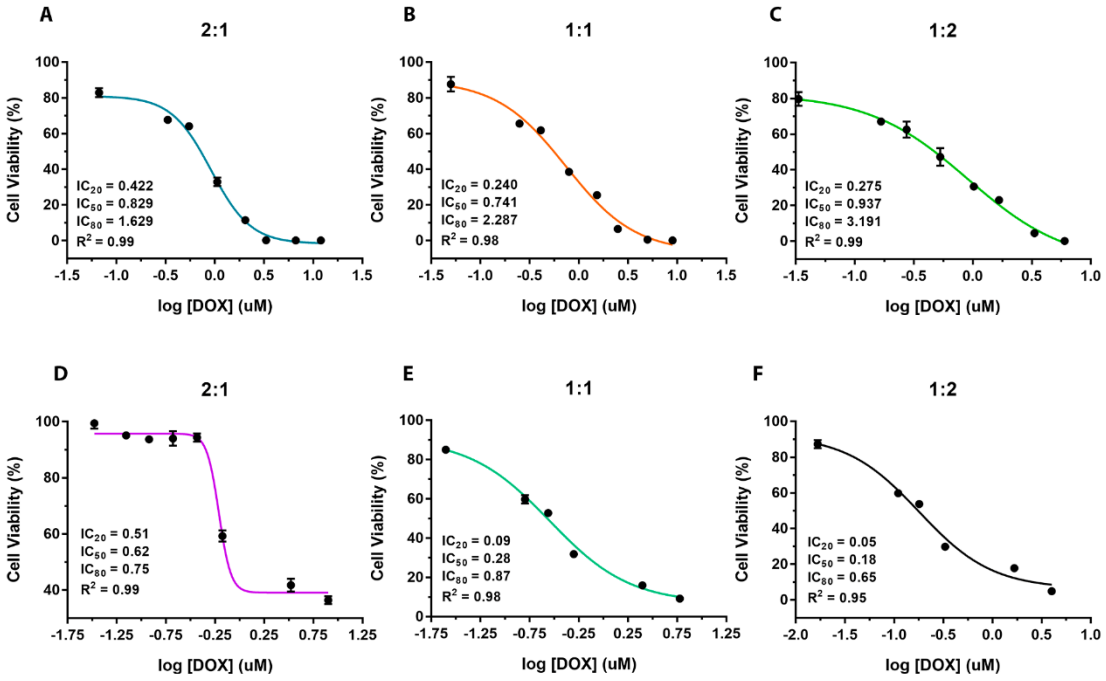


**Figure 10 -** Comparison of the DOX:AO combinations (2:1, 1:1 and 1:2) effect in HeLa (A - C) and MCF-7 (D - F) cells. Dose-response curves of 2DOX:1AO (A and D), 1DOX:1AO (B and E) and 1DOX:2AO (C and F) and respective ICs values; Data are presented as mean ± s.d., n = 5.

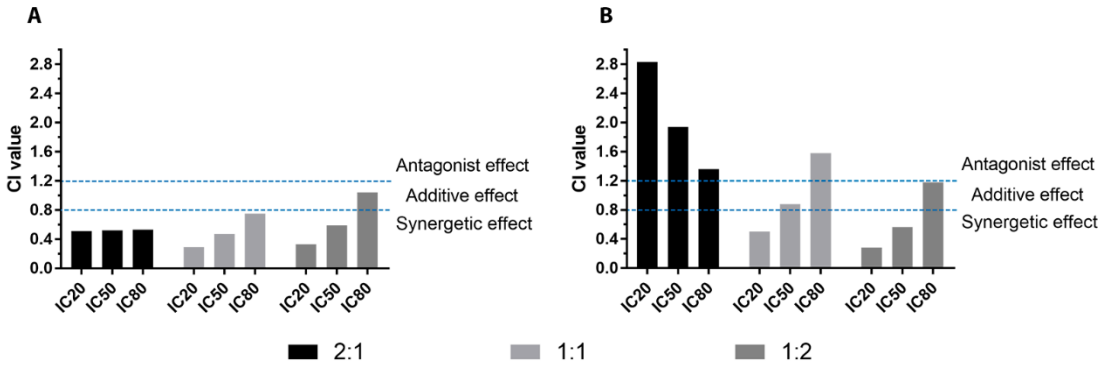


**Figure 11 -** Chou-Talay analysis for 2:1, 1:1, and 1:2 ratios of DOX:AO in (A) HeLa and (B) MCF-7 cells. CI values of CI < 0.8, 0.8 < CI < 1.2 and CI > 1.2 were consider synergistic, addictive and antagonistic effects, respectively.

## 3.3. Synthesis and characterization of TPANIS

The PEG is a hydrophilic polymer that can increase the nanoparticles' blood circulation time, block the formation of the protein corona, and improve colloidal stability [61, 147, 148]. On the other side, ANIS is a ligand with a small molecular weight with a high

affinity to the sigma receptor. This receptor is overexpressed on the surface of a wide number of human cancers, such as neuroblastomas, glioma, melanoma, breast, prostate, and lung cancer. Therefore, this ligand can improve the nanoparticles' selectivity to cancer cells reducing the nonspecific distribution [147, 149, 150]. With that in mind, ANIS was chemically grafted to PEG (PANIS) via a CDI-mediated coupling reaction [151, 152]. Then, the resulting polymer was reacted with TESPIC (TPANIS), a hydrogen-transfer nucleophilic addition reaction, to allow its grafting to the AuMSS surface (Figure 12 A).

The TESPIC-PEG-ANIS modification was followed step-by-step through FTIR analysis (Figure 12 B). The FTIR spectra of PEG present the characteristics peaks around 2800 $cm^{-1}$ and 1000 - 1200 $cm^{-1}$ region corresponding to the stretching vibrations of C-H and C-O, respectively [153]. Furthermore, the FTIR spectrum of PANIS shows both the PEG characteristic peaks and the ANIS C-O-C vibration peak in the 1500 - 1650 $cm^{-1}$ region. Otherwise, the TPANIS spectrum also showed the TESPIC characteristic peaks at the 800 $cm^{-1}$ region attributed to Si-O-C and Si-C bonds.

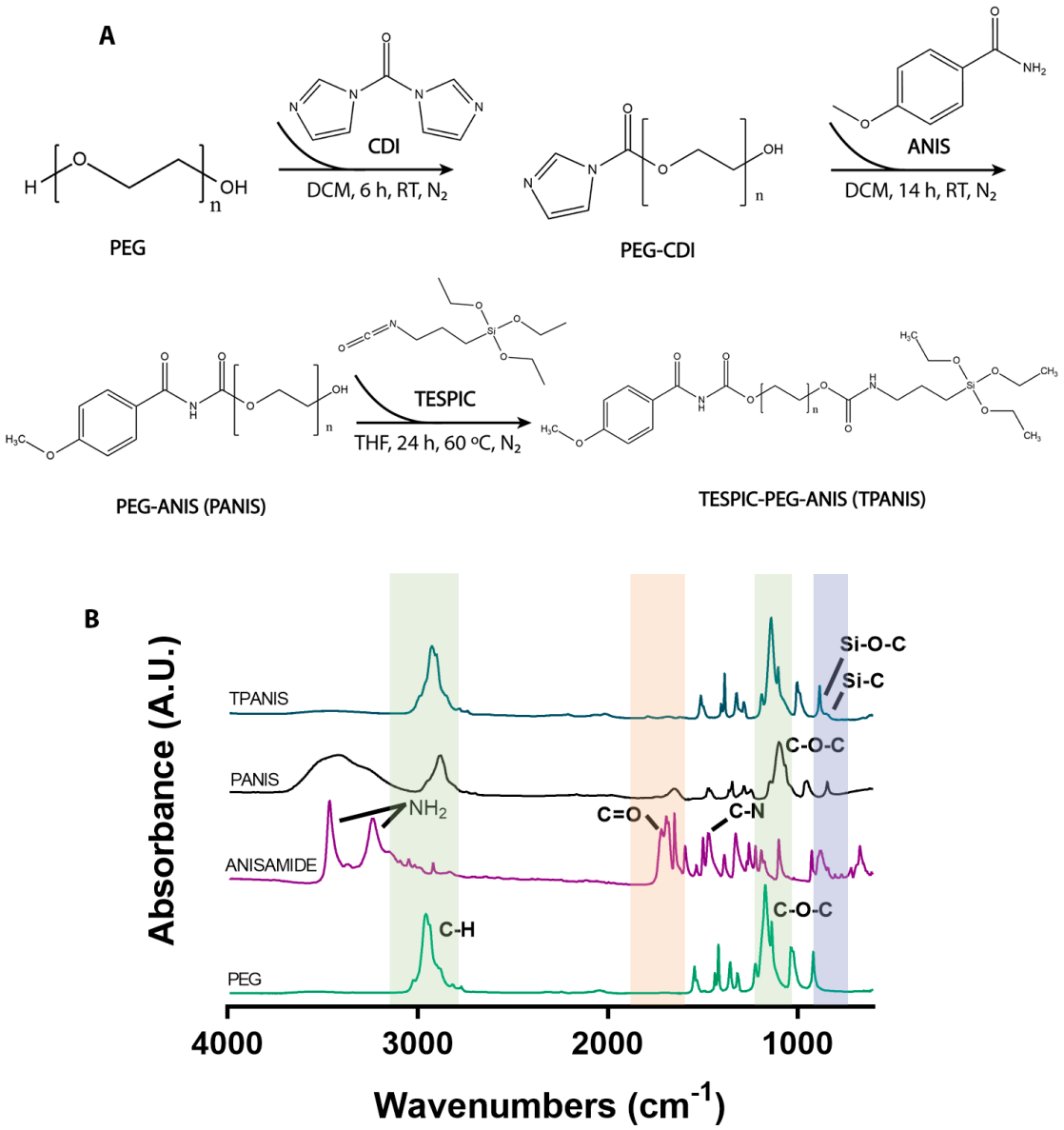


**Figure 12 -** Synthesis and characterization of TPANIS. (A) Representation of the synthesis process of TPANIS. (B) FTIR spectra of PEG, ANIS, PANIS, and TPANIS polymers.

## 3.4. Synthesis and characterization of AuMSS nanospheres

The AuMSS nanospheres were produced using a one-pot procedure previously described in the literature [132]. This process can be divided into two main phases, the spherical gold cores production and the coating with a mesoporous silica shell. Initially, CTAB-stabilized gold nanospheres are produced by promoting the reduction of the gold precursor ($HAuCl_4$) in an alkaline solution containing CTAB and formaldehyde. Then, TEOS is added to the gold nanospheres to originate the mesoporous silica shell. During this reaction, the TEOS molecule is hydrolyzed (*i.e.* removal of the TEOS alkoxy group) and starts to condensate around the gold core using the CTAB micelles as templates for the mesopores [119]. Afterward, the cytotoxic CTAB molecules are removed via a solvent

extraction protocol that uses an acid/alcohol mixture [119, 131]. The nanoparticles organization in core-shell structure allows the combination of the properties of its materials, *i.e.* bioimaging of the gold-core and drug delivery of the mesoporous silica. In this way, the successful synthesis of AuMSS nanoparticles and its core-shell organization was evaluated by TEM. In Figure 13 A and B, it is possible to observe the particle organization in a gold core (darker central region of the nanoparticles) coated with a uniform mesoporous silica shell. Furthermore, the DLS data (Figure 13 C and D) shows that the AuMSS nanospheres are homogeneous and present an average diameter of 117.2 ± 1.7 nm. Moreover, after the functionalization of AuMSS nanospheres with TPANIS is observed an increase in particles hydrodynamic diameter to 192.6 ± 2.9 nm (Figure 13 D). This result indicates the successful grafting of TPANIS on the surface of AuMSS nanospheres. Further, it is important to notice that the obtained mean sizes are still within the range considered ideal for application in blood circulation, allowing the nanoparticles to take advantage of the EPR effect, which consequently enable their passive accumulation in the tumor tissue tumor [131].

The surface charge of AuMSS nanoformulations was also measured to characterize the surface functionalization of the nanoparticles (Figure 14 A). The obtained results show the characteristic negative surface charge of AuMSS nanomaterials (- 28.1 ± 0.6 mV), which is justified by the presence of negatively charged silanol groups on the surface of mesoporous silica. Otherwise, the AuMSS-TPANIS nanospheres presented a slightly less negative surface charge (- 24.7 ± 0.4 mV). As already mentioned, the nanoparticles' zeta potential is an important parameter since it affects the nanoparticle interaction with the biological components, influencing the nanoparticle pharmacokinetic profile, blood circulation time, and biocompatibility [72, 154]. Despite a neutral surface charge (zeta potential of ± 10 mV) often being considered the ideal for biological applications, slightly negative nanoparticles usually presented increased blood circulation times, since their interactions with blood cellular components and serum proteins are decreased [72].

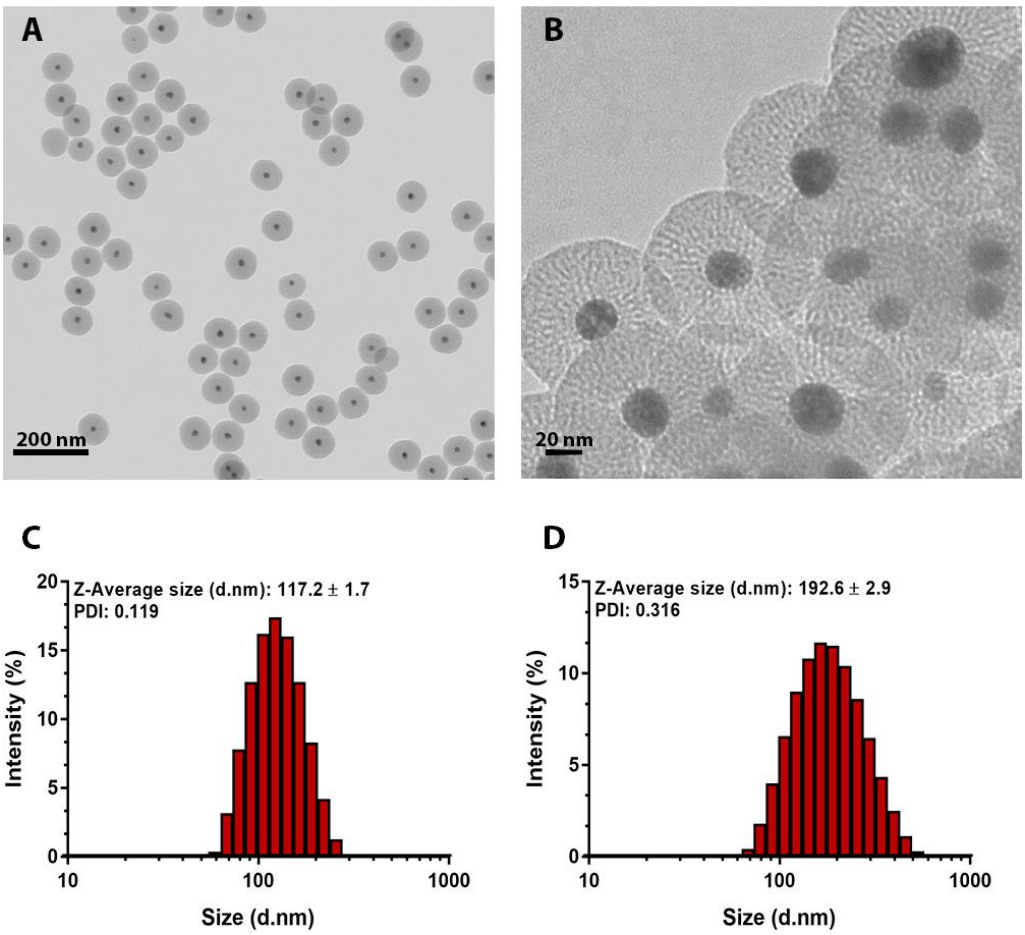


**Figure 13 -** Analysis of the morphology and size distribution of AuMSS nanoformulations. TEM images of AuMSS (A) and AuMSS-TPANIS (B) nanospheres. DLS size distribution (number/intensity) of AuMSS (C) and AuMSS-TPANIS (D) nanospheres. Data are presented as mean ± s.d., n = 3.

The FTIR characterization of the AuMSS nanoformulations was carried out for assessing the formation of the mesoporous silica coating, the efficacy of the purification procedure, and the successful functionalization with TPANIS (Figure 14 B). The FTIR spectra of AuMSS shows three characteristic peaks of mesoporous silica in 1300 to 740 $cm^{-1}$ region that corresponds to Si-O-Si, Si-OH, and Si-O vibrations. Further, the non-purified AuMSS also presents the characteristic peaks of CTAB, namely the C-H stretching vibrations observed at 2923 and 2855 $cm^{-1}$. After the purification procedure, the previous C-H peaks attributed to CTAB completely disappeared, which indicates the complete removal of the cytotoxic CTAB molecules. Otherwise, after the grafting of TPANIS to the AuMSS nanospheres it was possible to observe the presence of additional peaks corresponding to the TPANIS polymer, such as the stretching vibrations of C-H at ≈2800 $cm^{-1}$ and C-O-C vibration peaks in the 1500 - 1650 $cm^{-1}$ region. Additionally, the AuMSS-TPANIS polymeric content was determined by TGA, as shown in Figure 14 C. As expected, the weight losses registered for non-coated AuMSS nanospheres were minimal (3 - 4%). Such is justified by the inorganic nature of AuMSS nanospheres were this small

weight change can be attributed to the loss of the hydroxyl groups on the external surface of the particles or the evaporation of water adsorbed in the interior region of the mesopores. On the other side, the AuMSS-TPANIS presented a weight loss of 24% due to the polymer pyrolysis. Overall, the different physicochemical results corroborate the successful immobilization of TPANIS on the AuMSS surface.

To further assess the advantages of the TPANIS coating, size analysis were performed to the different AuMSS formulations after dispersion in water for different periods (Figure 14 D). The obtained results demonstrate that the AuMSS-TPANIS present a similar size and no signs of aggregation were detected during the experiment. Contrarily, the non-coated AuMSS nanospheres showed a size increase from ≈115 to ≈165 nm with the incubation in water. Such findings further attest the successful functionalization of AuMSS nanospheres with the TPANIS and support the applicability of this nanosystem in the following experiments.

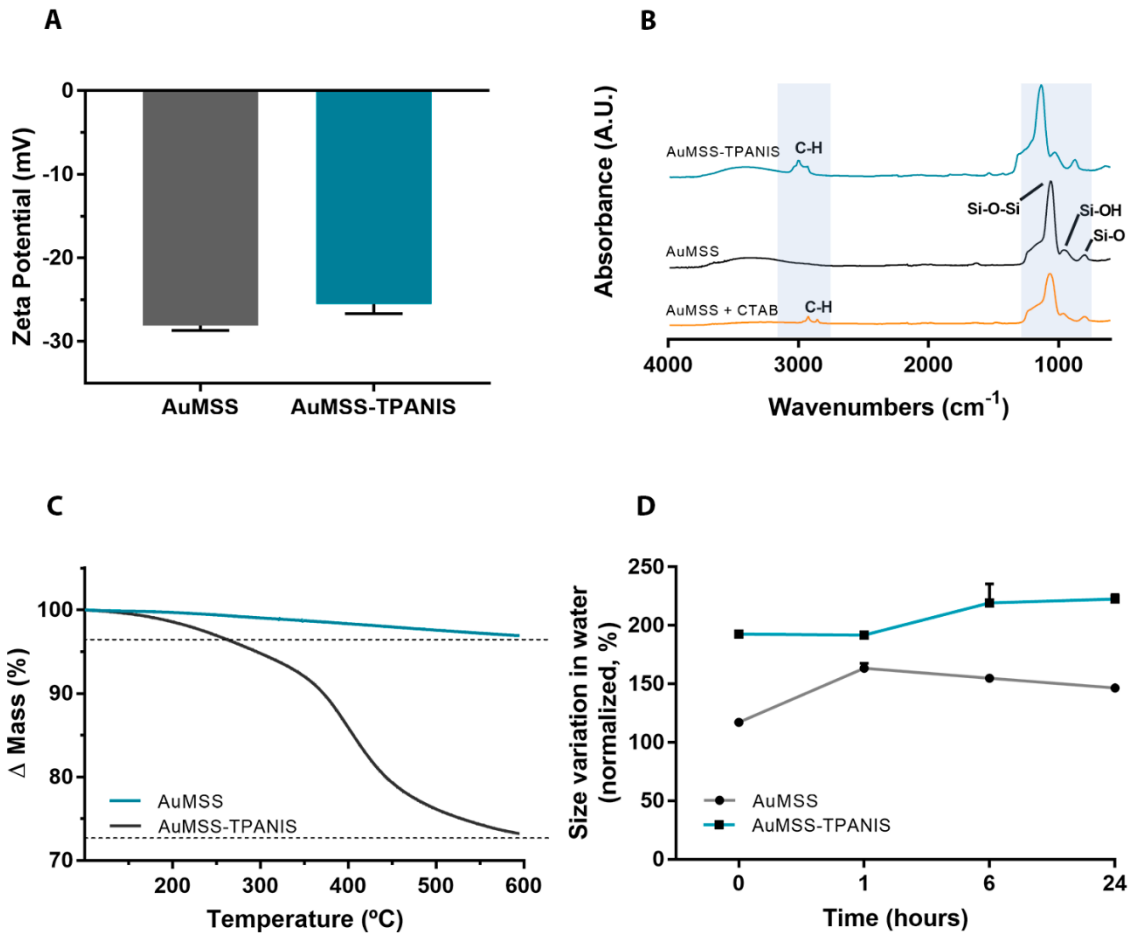


**Figure 14** - Physicochemical characterization of AuMSS nanoformulations. (A) Surface charge analysis of AuMSS and AuMSS-TPANIS nanospheres, n = 3. (B) FTIR spectra of non-purified (AuMSS + CTAB), AuMSS, and AuMSS-TPANIS nanospheres. (C) TGA analysis of AuMSS and AuMSS-TPANIS nanospheres. (D) Size variation of AuMSS and AuMSS-TPANIS nanospheres when dispersed in ultrapure water for 24 h. Data are presented as mean ± s.d., n = 3.

## 3.5. Drug loading capacity of AuMSS and AuMSS-TPANIS

The AuMSS capacity to encapsulate chemotherapeutic drugs was characterized by measuring the E.E of DOX and AO. The loading was promoted by resuspending the AuMSS in the DOX or AO solution for 48 h (Figure 15 A). The obtained results showed that all the AuMSS formulations can encapsulate the two drugs. The non-coated AuMSS nanospheres presented an E.E of 92% for DOX and 48% for AO (Figure 15 B). Otherwise, the AuMSS-TPANIS nanospheres presented a slightly higher E.E, 97% for DOX and 53% for AO. The drug loading in the AuMSS nanoparticles is mediated by the establishment of electrostatic and/or hydrophobic interactions between the drug molecules and the silica mesopores. The increase in the E.E with the TPANIS functionalization can be justified by the additional entrapment of drug molecules at the particle surface promoted by the TPANIS polymer.

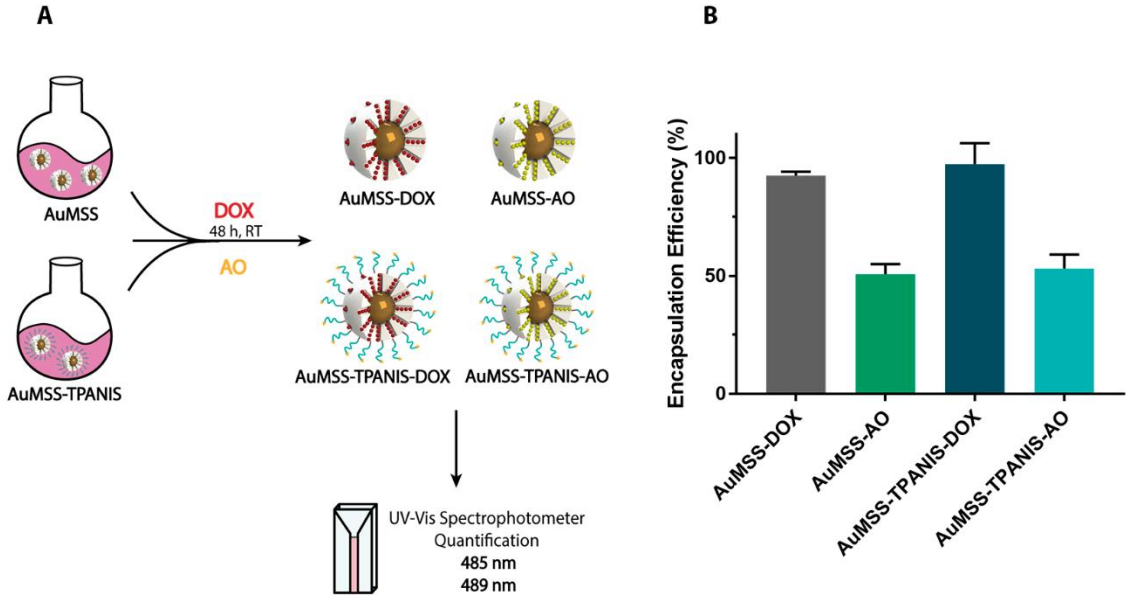


**Figure 15 -** Characterization of the DOX and AO encapsulation efficiency. (A) Schematics of DOX or AO loading in AuMSS and AuMSS-TPANIS nanoparticles. (B) DOX and AO encapsulation efficiency on AuMSS and AuMSS-TPANIS nanospheres. Data are presented as mean ± s.d, n = 3.

## 3.6. Nanoparticles biocompatibility

### 3.6.1. Cell viability

The biocompatibility of AuMSS nanospheres and coated with TPANIS was evaluated with HeLa, MCF-7, and FibH cells through the resazurin assay. For that purpose, the two different AuMSS formulations were incubated with the cells for 24, 48, and 72 h, at concentrations ranging from 25 to 200 μg/mL (Figure 16). According to the ISO 10993-5, a material has a cytotoxic effect when the cell viability suffers a reduction of more than 30%. The obtained results reveal that both the AuMSS and AuMSS-TPANIS nanospheres

did not induce a cytotoxic effect in the three tested cell lines, registering cell viabilities superior to 70%, even at the highest concentration (200 μg/mL). These results are in agreement with the results described in the literature for AuMSS-based nanosystems and the safety profile of PEG (FDA-approved for biomedical applications).

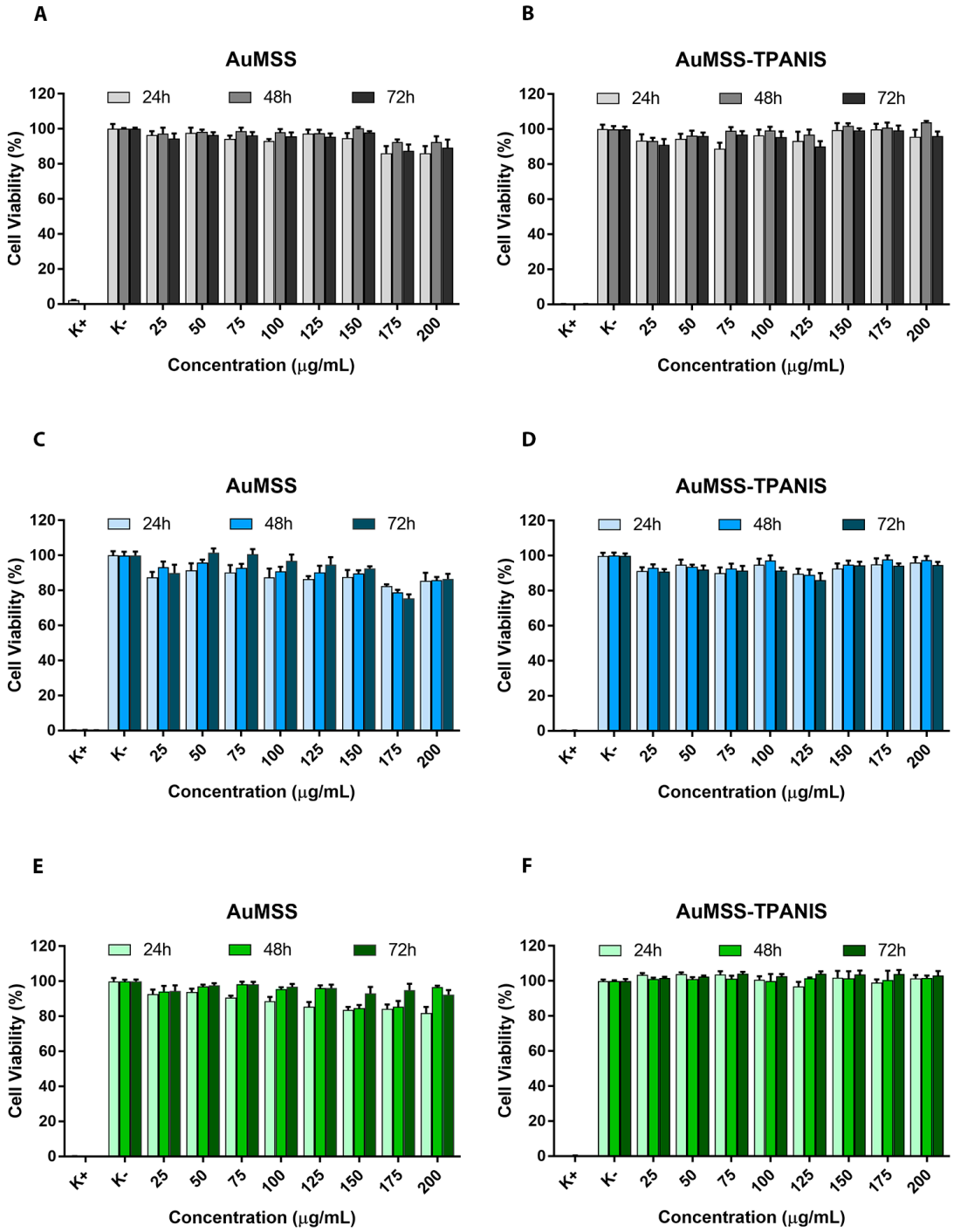


**Figure 16 -** Evaluation of AuMSS and AuMSS-TPANIS cytocompatibility in HeLa (A, B), MCF-7 (C, D) and FibH (E, F) at 24, 48, and 72 h. Cytocompatibility analysis for AuMSS (A, C, E) and AuMSS-TPANIS nanospheres (B, D, F). Positive control ($K^+$): cells treated with EtOH; Negative control ($K^-$): cells without nanoparticles incubation. Data are presented as mean ± s.d., n = 5.

## 3.7. AuMSS spheres cellular uptake

After assessing the biocompatibility of AuMSS nanoformulations, the nanoparticles' cellular uptake was evaluated by fluorescence spectroscopy. For that purpose, FITC-stained AuMSS and AuMSS-TPANIS nanospheres were incubated with FibH (healthy cells with low expression of sigma receptors), HeLa (cancer cells with low expression of sigma receptors), and MCF-7 (cancer cells overexpressing sigma receptors) cells for 4 h (Figure 17 A). These different cell lines were selected to evaluate the ANIS targeting ability. The fluorescence spectroscopy studies revealed that the AuMSS nanospheres functionalization with TPANIS improves the nanoparticle uptake in MCF-7 cancer cells, 326 ± 119% when compared to non-coated AuMSS nanospheres. Otherwise, in HeLa and FibH cells, the AuMSS-TPANIS presented an uptake similar to non-coated AuMSS nanospheres. This enhanced AuMSS-TPANIS uptake in MCF-7 cells indicates that the nanoparticle internalization may be mediated by the ANIS interaction with the sigma receptors overexpressed in this cell line. With that in mind, the uptake experiments were repeated by performing the pre-treatment of FibH, HeLa, and MCF-7 cells with free ANIS for 3 h before the nanoparticle incubation. The obtained data demonstrated that the pre-treatment with ANIS results in a similar AuMSS-TPANIS uptake in the 3 tested cell lines. Therefore, this experiment demonstrated that the introduction of TPANIS in the AuMSS nanospheres confer to the nanoparticles a preferential uptake in cancer cells overexpressing the sigma receptors, such as breast cancer, melanoma, and prostate cancer [149].

## 3.8. Cytotoxic effect of loaded AuMSS-TPANIS spheres

The anti-cancer potential of DOX or AO loaded AuMSS-TPANIS nanospheres was evaluated in HeLa and MCF-7 cells. For that purpose, the cancer cells were incubated with AuMSS-TPANIS nanospheres (maximum nanoparticle concentration of 200 μg/mL corresponding to DOX:AO drug ratios of 2:1, 1:1, and 1:2) for 48 h. The obtained results (Figure 17 B) show that the AuMSS-TPANIS nanospheres have a superior cytotoxic effect on MCF-7 cells, 49%, 45%, and 41% of viable cells for the DOX:AO ratio of 2:1, 1:1, and 1:2, respectively. In contrast, the HeLa cells presented viabilities around 90% after the treatment with drug-loaded AuMSS-TPANIS nanospheres. Such difference can be attributed to the Anisamide-mediated active targeting towards MCF-7 cancer cells, which increases the nanoparticle uptake in this cell line maximizing the therapeutic effect.

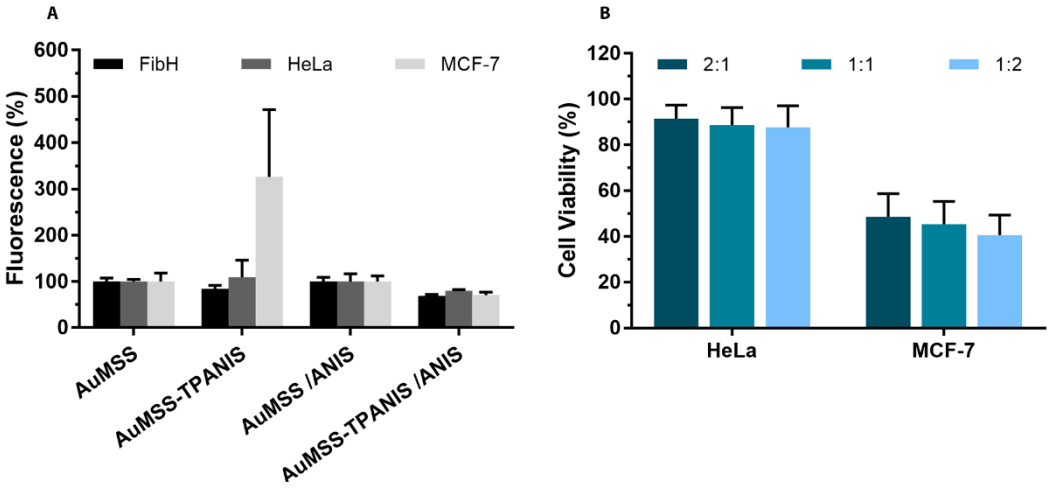


**Figure 17** - Analysis of AuMSS and AuMSS-TPANIS cellular uptake and cytotoxic effect. (A) Fluorescence spectroscopy analysis of the AuMSS and AuMSS-TPANIS uptake by FibH, HeLa, and MCF-7 cells with or without pre-treatment with Anisamide (ANIS). (B) Cytotoxic activity of AuMSS and AuMSS-TPANIS nanospheres at DOX:AO ratio of 2:1, 1:1, and 1:2. Data are presented as mean ± s.d., n = 5.

# Chapter 4

# Conclusions and Future Perspectives

# 4. Conclusions and Future Perspectives

Nowadays, cancer remains a major public health problem in the world, causing millions of deaths every year. Among the available therapeutic approaches, chemotherapy is the first line of treatment. Nevertheless, chemotherapeutic drugs present several disadvantages that affect the therapeutic outcome, such as poor solubility, lack of selectivity, and pronounced side effects. Thus, there is a huge demand to develop novel and more effective therapeutic approaches to improve the efficacy of anticancer treatments. Combinatorial therapies based on the simultaneous administration of multiple drugs intend to overcome the limitations of conventional chemotherapy by targeting simultaneously different metabolic pathways to create additive or synergetic effects that potentiate the therapeutic efficacy even at smaller drug doses.

Taking this into account, this dissertation aimed to design a dual drug combination (DOX and AO) to be encapsulated in AuMSS nanospheres. Moreover, a novel AuMSS surface modification based on TPANIS was developed to improve nanoparticles' blood circulation time and specificity to cancer cells. The obtained results demonstrated that the DOX:AO drug combination can mediate a synergistic therapeutic effect in both HeLa and MCF-7 cells, particularly at the 2:1, 1:1, and 1:2 ratios. Otherwise, AuMSS nanoparticles' functionalization with the TPANIS promoted a slight increase in the nanoparticles' size and stability. The successful incorporation of the polymers on nanoparticles surface was also confirmed by TGA and by FTIR. Additionally, both the DOX and AO were successfully encapsulated on the AuMSS-TPANIS nanospheres. In *in vitro* studies, nanoparticles demonstrated to be biocompatible when in contact with healthy cells (fibroblasts) and cancer cells (HeLa and MCF-7) up to the maximum tested concentration of 200 μg/mL. Moreover, the AuMSS nanospheres' functionalization with TPANIS significantly increased their internalization by MCF-7 cells. This selectivity towards MCF-7 (overexpressing sigma receptors) also resulted in an enhanced cytotoxic effect against this cell line. Overall, these results demonstrated the therapeutic potential of the DOX:AO drug combination as well as the targeting capacity of AuMSS-TPANIS nanospheres, which can render a superior anticancer efficacy.

In the future, the TPANIS polymer capacity to control the DOX and AO release profile from AuMSS-TPANIS nanospheres will be characterized at physiological and acidic pH. Moreover, additional biocompatibility assays (*e.g* hemolysis profile) will be performed to confirm the enhanced biological performance of AuMSS-TPANIS. Furthermore, the anti-cancer potential of the DOX:AO combination mediated by the AuMSS-TPANIS will be also characterized in 3D cell culture models. Finally, *in vivo* assays will allow to

evaluate the TPANIS potential to improve the biodistribution and selectivity of the AuMSS nanospheres as well as to characterize its biosafety and anti-tumoral effect.

# Chapter 5

# References

# 5. References


1. Siegel, R.L., K.D. Miller, and A. Jemal, *Cancer statistics, 2019.* CA: A Cancer Journal for Clinicians, 2019. **69**(1): p. 7-34.
2. Santaballa, A., et al., *SEOM clinical guideline for secondary prevention (2019).* Clinical and Translational Oncology, 2020. **22**(2): p. 187-192.
3. Siegel, R.L., K.D. Miller, and A. Jemal, *Cancer statistics, 2020.* CA: A Cancer Journal for Clinicians, 2020. **70**(1): p. 7-30.
4. Miranda, N.G., Margarida Brito; Andrade, Carla; Santos, Gonçalo, *Programa Nacional para as Doenças Oncológicas 2017.* Direção Geral de Saúde, 2017.
5. Aslam, M.S., et al., *Side Effects of Chemotherapy in Cancer Patients and Evaluation of Patients Opinion about Starvation Based Differential Chemotherapy.* Journal of Cancer Therapy, 2014. **5**: p. 6.
6. Lee, J.J., L. Saiful Yazan, and C.A. Che Abdullah, *A review on current nanomaterials and their drug conjugate for targeted breast cancer treatment.* International journal of nanomedicine, 2017. **12**: p. 2373-2384.
7. Malandrino, A., et al., *Complex mechanics of the heterogeneous extracellular matrix in cancer.* Extreme Mechanics Letters, 2018. **21**: p. 25-34.
8. Arneth, B., *Tumor Microenvironment.* Medicina, 2020. **56**(1).
9. Roma-Rodrigues, C., et al., *Targeting Tumor Microenvironment for Cancer Therapy.* International Journal of Molecular Sciences, 2019. **20**(4).
10. Nisticò, P. and G. Ciliberto, *Biological mechanisms linked to inflammation in cancer: Discovery of tumor microenvironment-related biomarkers and their clinical application in solid tumors.* The International Journal of Biological Markers, 2020. **35**: p. 8-11.
11. Papaccio, F., et al., *Concise Review: Cancer Cells, Cancer Stem Cells, and Mesenchymal Stem Cells: Influence in Cancer Development.* STEM CELLS Translational Medicine, 2017. **6**(12): p. 2115-2125.
12. Liu, J., et al., *Nanomedicine for tumor microenvironment modulation and cancer treatment enhancement.* Nano Today, 2018. **21**: p. 55-73.
13. Costa, E.C., et al., *3D tumor spheroids: an overview on the tools and techniques used for their analysis.* Biotechnology Advances, 2016. **34**(8): p. 1427-1441.
14. Trédan, O., et al., *Drug Resistance and the Solid Tumor Microenvironment.* JNCI: Journal of the National Cancer Institute, 2007. **99**(19): p. 1441-1454.
15. Fouad, Y.A. and C. Aanei, *Revisiting the hallmarks of cancer.* American Journal of Cancer Research, 2017. **7**(5): p. 1016-1036.
16. Hanahan, D. and Robert A. Weinberg, *Hallmarks of Cancer: The Next Generation.* Cell, 2011. **144**(5): p. 646-674.
17. Oltean, S. and D.O. Bates, *Hallmarks of alternative splicing in cancer.* Oncogene, 2014. **33**(46): p. 5311-5318.
18. Di Fiore, R., et al., *RB1 in cancer: Different mechanisms of RB1 inactivation and alterations of pRb pathway in tumorigenesis.* Journal of Cellular Physiology, 2013. **228**(8): p. 1676-1687.
19. Shay, J.W., et al., *Telomerase and cancer.* Human Molecular Genetics, 2001. **10**(7): p. 677-685.
20. Akincilar, S.C., B. Unal, and V. Tergaonkar, *Reactivation of telomerase in cancer.* Cellular and Molecular Life Sciences, 2016. **73**(8): p. 1659-1670.
21. Kalluri, R., *Basement membranes: structure, assembly and role in tumour angiogenesis.* Nature Reviews Cancer, 2003. **3**(6): p. 422-433.

22. Nishida, N., et al., *Angiogenesis in cancer.* Vascular health and risk management, 2006. **2**(3): p. 213-219.
23. Gout, S. and J. Huot, *Role of Cancer Microenvironment in Metastasis: Focus on Colon Cancer.* Cancer Microenvironment, 2008. **1**(1): p. 69-83.
24. Miller, K.D., et al., *Cancer treatment and survivorship statistics, 2019.* CA: A Cancer Journal for Clinicians, 2019. **69**(5): p. 363-385.
25. Rescigno, M., F. Avogadri, and G. Curigliano, *Challenges and prospects of immunotherapy as cancer treatment.* Biochimica et Biophysica Acta (BBA) - Reviews on Cancer, 2007. **1776**(1): p. 108-123.
26. Ravnikar, V.A., *Compliance with hormone therapy.* American Journal of Obstetrics and Gynecology, 1987. **156**(5): p. 1332-1334.
27. Delaney, G., et al., *The role of radiotherapy in cancer treatment.* Cancer, 2005. **104**(6): p. 1129-1137.
28. Xu, X., et al., *Cancer nanomedicine: from targeted delivery to combination therapy.* Trends in Molecular Medicine, 2015. **21**(4): p. 223-232.
29. Coffey, J.C., et al., *Excisional surgery for cancer cure: therapy at a cost.* The Lancet Oncology, 2003. **4**(12): p. 760-768.
30. Senapati, S., et al., *Controlled drug delivery vehicles for cancer treatment and their performance.* Signal Transduction and Targeted Therapy, 2018. **3**(1): p. 7.
31. Krukiewicz, K. and J.K. Zak, *Biomaterial-based regional chemotherapy: Local anticancer drug delivery to enhance chemotherapy and minimize its side-effects.* Materials Science and Engineering: C, 2016. **62**: p. 927-942.
32. Nial, J.W., et al., *DNA Intercalators in Cancer Therapy: Organic and Inorganic Drugs and Their Spectroscopic Tools of Analysis.* Mini Reviews in Medicinal Chemistry, 2007. **7**(6): p. 627-648.
33. Hossen, S., et al., *Smart nanocarrier-based drug delivery systems for cancer therapy and toxicity studies: A review.* Journal of Advanced Research, 2019. **15**: p. 1-18.
34. Huang, Y., et al., *Applications of nanoparticle drug delivery systems for the reversal of multidrug resistance in cancer.* Oncology letters, 2016. **12**(1): p. 11-15.
35. Kapse-Mistry, S., et al., *Nanodrug delivery in reversing multidrug resistance in cancer cells.* Frontiers in Pharmacology, 2014. **5**: p. 159.
36. Wu, C.-P., C.-H. Hsieh, and Y.-S. Wu, *The Emergence of Drug Transporter-Mediated Multidrug Resistance to Cancer Chemotherapy.* Molecular Pharmaceutics, 2011. **8**(6): p. 1996-2011.
37. Kelley, M.R., D. Logsdon, and M.L. Fishel, *Targeting DNA repair pathways for cancer treatment: what's new?* Future oncology (London, England), 2014. **10**(7): p. 1215-1237.
38. Zaal, E.A. and C.R. Berkers, *The Influence of Metabolism on Drug Response in Cancer.* Frontiers in Oncology, 2018. **8**: p. 500.
39. Al-Lazikani, B., U. Banerji, and P. Workman, *Combinatorial drug therapy for cancer in the post-genomic era.* Nature Biotechnology, 2012. **30**(7): p. 679-692.
40. Bayat Mokhtari, R., et al., *Combination therapy in combating cancer.* Oncotarget, 2017. **8**(23): p. 38022-38043.
41. Zhang, R.X., et al., *Nanomedicine of synergistic drug combinations for cancer therapy – Strategies and perspectives.* Journal of Controlled Release, 2016. **240**: p. 489-503.

42. Hu, C.-M.J. and L. Zhang, *Nanoparticle-based combination therapy toward overcoming drug resistance in cancer.* Biochemical Pharmacology, 2012. **83**(8): p. 1104-1111.
43. O'Shaughnessy, J., et al., *Superior Survival With Capecitabine Plus Docetaxel Combination Therapy in Anthracycline-Pretreated Patients With Advanced Breast Cancer: Phase III Trial Results.* Journal of Clinical Oncology, 2002. **20**(12): p. 2812-2823.
44. Kosmas, C., et al., *Evaluation of the paclitaxel–ifosfamide–cisplatin (TIP) combination in relapsed and/or metastatic cervical cancer.* British Journal of Cancer, 2009. **101**(7): p. 1059-1065.
45. Ding, X., et al., *Optimized combinations of bortezomib, camptothecin, and doxorubicin show increased efficacy and reduced toxicity in treating oral cancer.* Anti-Cancer Drugs, 2015. **26**(5).
46. Wu, J., et al., *Functionalized MoS 2 nanosheet-capped periodic mesoporous organosilicas as a multifunctional platform for synergistic targeted chemo-photothermal therapy.* Chemical Engineering Journal, 2018. **342**: p. 90-102.
47. Thorn, C.F., et al., *Doxorubicin pathways: pharmacodynamics and adverse effects.* Pharmacogenetics and genomics, 2011. **21**(7): p. 440-446.
48. Zhu, H., et al., *Doxorubicin Redox Biology: Redox Cycling, Topoisomerase Inhibition, and Oxidative Stress.* Reactive oxygen species (Apex, N.C.), 2016. **1**(3): p. 189-198.
49. McGowan, J.V., et al., *Anthracycline Chemotherapy and Cardiotoxicity.* Cardiovascular Drugs and Therapy, 2017. **31**(1): p. 63-75.
50. Meredith, A.-M. and C.R. Dass, *Increasing role of the cancer chemotherapeutic doxorubicin in cellular metabolism.* Journal of Pharmacy and Pharmacology, 2016. **68**(6): p. 729-741.
51. Damiani, R.M., et al., *Pathways of cardiac toxicity: comparison between chemotherapeutic drugs doxorubicin and mitoxantrone.* Archives of Toxicology, 2016. **90**(9): p. 2063-2076.
52. Foucquier, J. and M. Guedj, *Analysis of drug combinations: current methodological landscape.* Pharmacology Research & Perspectives, 2015. **3**(3): p. e00149.
53. Lin, Y.-C., et al., *Acridine orange exhibits photodamage in human bladder cancer cells under blue light exposure.* Scientific Reports, 2017. **7**(1): p. 14103.
54. Kusuzaki, K., et al., *Acridine Orange could be an Innovative Anticancer Agent under Photon Energy.* In vivo, 2007. **21**: p. 205-14.
55. Iessi, E., et al., *Acridine Orange/exosomes increase the delivery and the effectiveness of Acridine Orange in human melanoma cells: A new prototype for theranostics of tumors.* Journal of Enzyme Inhibition and Medicinal Chemistry, 2017. **32**(1): p. 648-657.
56. Byvaltsev, V.A., et al. *Acridine Orange: A Review of Novel Applications for Surgical Cancer Imaging and Therapy*. Frontiers in Oncology, 2019. **9**, 925 DOI: 10.3389/fonc.2019.00925.
57. Pitchaimani, A., et al., *Photochemotherapeutic effects of UV-C on acridine orange in human breast cancer cells: potential application in anticancer therapy.* RSC Advances, 2014. **4**(42): p. 22123.
58. Liu, C.H., S.L. Sahoo, and M.H. Tsao, *Acridine orange coated magnetic nanoparticles for nucleus labeling and DNA adsorption.* Colloids Surfaces B: Biointerfaces, 2014. **115**: p. 150-6.

59. Bragagni, M., et al., *Synthesis of an acridine orange sulfonamide derivative with potent carbonic anhydrase IX inhibitory action.* J Enzyme Inhib Med Chem, 2017. **32**(1): p. 701-706.
60. Fotia, C., et al., *Acridine Orange is an Effective Anti-Cancer Drug that Affects Mitochondrial Function in Osteosarcoma Cells.* Curr Pharm Des, 2015. **21**(28): p. 4088-94.
61. Moreira, A.F., D.R. Dias, and I.J. Correia, *Stimuli-responsive mesoporous silica nanoparticles for cancer therapy: A review.* Microporous and Mesoporous Materials, 2016. **236**: p. 141-157.
62. Khot, L.R., et al., *Applications of nanomaterials in agricultural production and crop protection: A review.* Crop Protection, 2012. **35**: p. 64-70.
63. Liu, S., et al., *A review of extending performance of epoxy resins using carbon nanomaterials.* Composites Part B: Engineering, 2018. **136**: p. 197-214.
64. Makin, G., *Principles of chemotherapy.* Paediatrics and Child Health, 2018. **28**(4): p. 183-188.
65. Patra, J.K., et al., *Nano based drug delivery systems: recent developments and future prospects.* Journal of Nanobiotechnology, 2018. **16**(1): p. 71.
66. Hu, Q., et al., *Recent advances of cocktail chemotherapy by combination drug delivery systems.* Advanced Drug Delivery Reviews, 2016. **98**: p. 19-34.
67. Xin, Y., et al., *Nanoscale drug delivery for targeted chemotherapy.* Cancer Letters, 2016. **379**(1): p. 24-31.
68. Cao, J., et al., *Recent progress in synergistic chemotherapy and phototherapy by targeted drug delivery systems for cancer treatment.* Artificial Cells, Nanomedicine, and Biotechnology, 2018. **46**(sup1): p. 817-830.
69. Yildirimer, L., et al., *Toxicology and clinical potential of nanoparticles.* Nano today, 2011. **6**(6): p. 585-607.
70. Kim, T. and T. Hyeon, *Applications of inorganic nanoparticles as therapeutic agents.* Nanotechnology, 2013. **25**(1): p. 012001.
71. Muller, R.H. and C.M. Keck, *Challenges and solutions for the delivery of biotech drugs – a review of drug nanocrystal technology and lipid nanoparticles.* Journal of Biotechnology, 2004. **113**(1): p. 151-170.
72. Ernsting, M.J., et al., *Factors controlling the pharmacokinetics, biodistribution and intratumoral penetration of nanoparticles.* Journal of Controlled Release, 2013. **172**(3): p. 782-794.
73. Blanco, E., H. Shen, and M. Ferrari, *Principles of nanoparticle design for overcoming biological barriers to drug delivery.* Nat Biotechnol, 2015. **33**(9): p. 941-51.
74. Fan, Z., et al., *Engineering long-circulating nanomaterial delivery systems.* Current Opinion in Biotechnology, 2020. **66**: p. 131-139.
75. Danhier, F., O. Feron, and V. Préat, *To exploit the tumor microenvironment: Passive and active tumor targeting of nanocarriers for anti-cancer drug delivery.* Journal of Controlled Release, 2010. **148**(2): p. 135-146.
76. de Melo-Diogo, D., et al., *Strategies to Improve Cancer Photothermal Therapy Mediated by Nanomaterials.* Advanced Healthcare Materials, 2017. **6**(10): p. 1700073.
77. Longmire, M., P.L. Choyke, and H. Kobayashi, *Clearance properties of nano-sized particles and molecules as imaging agents: considerations and caveats.* Nanomedicine (London, England), 2008. **3**(5): p. 703-717.

78. Cataldi, M., et al., *Emerging Role of the Spleen in the Pharmacokinetics of Monoclonal Antibodies, Nanoparticles and Exosomes.* International journal of molecular sciences, 2017. **18**(6): p. 1249.
79. Huynh, N.T., et al., *The rise and rise of stealth nanocarriers for cancer therapy: passive versus active targeting.* Nanomedicine, 2010. **5**(9): p. 1415-1433.
80. Kou, L., et al., *The endocytosis and intracellular fate of nanomedicines: Implication for rational design.* Asian Journal of Pharmaceutical Sciences, 2013. **8**(1): p. 1-10.
81. Tee, J.K., et al., *Nanoparticles' interactions with vasculature in diseases.* Chemical Society Reviews, 2019. **48**(21): p. 5381-5407.
82. Truong, N.P., et al., *The importance of nanoparticle shape in cancer drug delivery.* Expert Opinion on Drug Delivery, 2015. **12**(1): p. 129-142.
83. Decuzzi, P., et al., *Size and shape effects in the biodistribution of intravascularly injected particles.* Journal of Controlled Release, 2010. **141**(3): p. 320-327.
84. Arnida, et al., *Geometry and surface characteristics of gold nanoparticles influence their biodistribution and uptake by macrophages.* European Journal of Pharmaceutics and Biopharmaceutics, 2011. **77**(3): p. 417-423.
85. Ma, N., et al., *Shape-Dependent Radiosensitization Effect of Gold Nanostructures in Cancer Radiotherapy: Comparison of Gold Nanoparticles, Nanospikes, and Nanorods.* ACS Applied Materials & Interfaces, 2017. **9**(15): p. 13037-13048.
86. Moreira, A.F., et al., *Gold-core silica shell nanoparticles application in imaging and therapy: A review.* Microporous and Mesoporous Materials, 2018. **270**: p. 168-179.
87. Matsumoto, Y., et al., *Vascular bursts enhance permeability of tumour blood vessels and improve nanoparticle delivery.* (1748-3395 (Electronic)).
88. Guimarães, R.S., et al., *Overview of stimuli-responsive mesoporous organosilica nanocarriers for drug delivery.* Pharmacological Research, 2020. **155**: p. 104742.
89. Ganta, S., et al., *A review of stimuli-responsive nanocarriers for drug and gene delivery.* Journal of Controlled Release, 2008. **126**(3): p. 187-204.
90. Bazban-Shotorbani, S., et al., *Revisiting structure-property relationship of pH-responsive polymers for drug delivery applications.* Journal of Controlled Release, 2017. **253**: p. 46-63.
91. Pham, S.H., Y. Choi, and J. Choi, *Stimuli-Responsive Nanomaterials for Application in Antitumor Therapy and Drug Delivery.* Pharmaceutics, 2020. **12**(7).
92. Mohammadi, M., et al., *Synthesis and investigation of dual pH- and temperature-responsive behaviour of poly[2-(dimethylamino)ethyl methacrylate]-grafted gold nanoparticles.* Applied Organometallic Chemistry, 2017. **31**(9): p. e3702.
93. Ayano, E., et al., *Poly (N-isopropylacrylamide)–PLA and PLA blend nanoparticles for temperature-controllable drug release and intracellular uptake.* Colloids and Surfaces B: Biointerfaces, 2012. **99**: p. 67-73.
94. Mori, T. and M. Maeda, *Temperature-Responsive Formation of Colloidal Nanoparticles from Poly(N-isopropylacrylamide) Grafted with Single-Stranded DNA.* Langmuir, 2004. **20**(2): p. 313-319.
95. Hamner, K.L., et al., *Using Temperature-Sensitive Smart Polymers to Regulate DNA-Mediated Nanoassembly and Encoded Nanocarrier Drug Release.* ACS Nano, 2013. **7**(8): p. 7011-7020.
96. Mo, R., et al., *ATP-triggered anticancer drug delivery.* Nature Communications, 2014. **5**(1): p. 3364.

97. He, X., et al., *Correction to ATP-Responsive Controlled Release System Using Aptamer-Functionalized Mesoporous Silica Nanoparticles.* Langmuir, 2013. **29**(1): p. 510-510.
98. Fleige, E., M.A. Quadir, and R. Haag, *Stimuli-responsive polymeric nanocarriers for the controlled transport of active compounds: Concepts and applications.* Advanced Drug Delivery Reviews, 2012. **64**(9): p. 866-884.
99. Paris, J.L., et al., *Polymer-Grafted Mesoporous Silica Nanoparticles as Ultrasound-Responsive Drug Carriers.* ACS Nano, 2015. **9**(11): p. 11023-33.
100. Cheng, R., et al., *Dual and multi-stimuli responsive polymeric nanoparticles for programmed site-specific drug delivery.* Biomaterials, 2013. **34**(14): p. 3647-3657.
101. Dilnawaz, F., S. Acharya, and S.K. Sahoo, *Recent trends of nanomedicinal approaches in clinics.* International Journal of Pharmaceutics, 2018. **538**(1): p. 263-278.
102. Wicki, A., et al., *Nanomedicine in cancer therapy: Challenges, opportunities, and clinical applications.* Journal of Controlled Release, 2015. **200**: p. 138-157.
103. Ghosh, P., et al., *Gold nanoparticles in delivery applications.* Advanced Drug Delivery Reviews, 2008. **60**(11): p. 1307-1315.
104. Lohse, S.E. and C.J. Murphy, *The Quest for Shape Control: A History of Gold Nanorod Synthesis.* Chemistry of Materials, 2013. **25**(8): p. 1250-1261.
105. Huang, X. and M.A. El-Sayed, *Gold nanoparticles: Optical properties and implementations in cancer diagnosis and photothermal therapy.* Journal of Advanced Research, 2010. **1**(1): p. 13-28.
106. Her, S., D.A. Jaffray, and C. Allen, *Gold nanoparticles for applications in cancer radiotherapy: Mechanisms and recent advancements.* Advanced Drug Delivery Reviews, 2017. **109**: p. 84-101.
107. Sperling, R.A., et al., *Biological applications of gold nanoparticles.* Chemical Society Reviews, 2008. **37**(9): p. 1896-1908.
108. Chen, Y., Y. Xianyu, and X. Jiang, *Surface Modification of Gold Nanoparticles with Small Molecules for Biochemical Analysis.* Accounts of Chemical Research, 2017. **50**(2): p. 310-319.
109. Nath, S., et al., *Dextran-Coated Gold Nanoparticles for the Assessment of Antimicrobial Susceptibility.* Analytical Chemistry, 2008. **80**(4): p. 1033-1038.
110. Martínez-Torres, A.C., et al., *Chitosan gold nanoparticles induce cell death in HeLa and MCF-7 cells through reactive oxygen species production.* International journal of nanomedicine, 2018. **13**: p. 3235-3250.
111. Dreaden, E.C., et al., *The golden age: gold nanoparticles for biomedicine.* Chemical Society Reviews, 2012. **41**(7): p. 2740-2779.
112. Silva, A.S., et al., *Nanogold POxylation: towards always-on fluorescent lung cancer targeting.* RSC Advances, 2016. **6**(40): p. 33631-33635.
113. Zhang, X.-D., et al., *Size-dependent radiosensitization of PEG-coated gold nanoparticles for cancer radiation therapy.* Biomaterials, 2012. **33**(27): p. 6408-6419.
114. Bharti, C., et al., *Mesoporous silica nanoparticles in target drug delivery system: A review.* International journal of pharmaceutical investigation, 2015. **5**(3): p. 124-133.
115. Jafari, S., et al., *Mesoporous silica nanoparticles for therapeutic/diagnostic applications.* Biomedicine & Pharmacotherapy, 2019. **109**: p. 1100-1111.
116. Karimi, M., et al., *Smart micro/nanoparticles in stimulus-responsive drug/gene delivery systems.* Chemical Society reviews, 2016. **45**(5): p. 1457-1501.

117. Castillo, R.R., et al., *Advances in mesoporous silica nanoparticles for targeted stimuli-responsive drug delivery: an update.* Expert opinion on drug delivery, 2019. **16**(4): p. 415-439.
118. Dias, D.R., A.F. Moreira, and I.J. Correia, *The effect of the shape of gold core–mesoporous silica shell nanoparticles on the cellular behavior and tumor spheroid penetration.* Journal of Materials Chemistry B, 2016. **4**(47): p. 7630-7640.
119. Chen, J., et al., *One-pot synthesis of thermally stable gold@mesoporous silica core-shell nanospheres with catalytic activity.* Nano Research, 2013. **6**(12): p. 871-879.
120. Vazquez, N.I., et al., *Synthesis of mesoporous silica nanoparticles by sol–gel as nanocontainer for future drug delivery applications.* Boletín de la Sociedad Española de Cerámica y Vidrio, 2017. **56**(3): p. 139-145.
121. Vigderman, L., B.P. Khanal, and E.R. Zubarev, *Functional Gold Nanorods: Synthesis, Self-Assembly, and Sensing Applications.* Advanced Materials, 2012. **24**(36): p. 4811-4841.
122. Huang, X., et al., *Cancer Cell Imaging and Photothermal Therapy in the Near-Infrared Region by Using Gold Nanorods.* Journal of the American Chemical Society, 2006. **128**(6): p. 2115-2120.
123. An, L., et al., *Small Gold Nanorods: Recent Advances in Synthesis, Biological Imaging, and Cancer Therapy.* Materials, 2017. **10**(12).
124. Wang, S., et al., *Biologically Inspired Polydopamine Capped Gold Nanorods for Drug Delivery and Light-Mediated Cancer Therapy.* ACS Applied Materials & Interfaces, 2016. **8**(37): p. 24368-24384.
125. Rodrigues, C.F., et al., *Functionalization of AuMSS nanorods towards more effective cancer therapies.* Nano Research, 2019. **12**(4): p. 719-732.
126. Barbosa, S., et al., *Tuning Size and Sensing Properties in Colloidal Gold Nanostars.* Langmuir, 2010. **26**(18): p. 14943-14950.
127. Skrabalak, S.E., et al., *Gold Nanocages: Synthesis, Properties, and Applications.* Accounts of Chemical Research, 2008. **41**(12): p. 1587-1595.
128. Cheheltani, R., et al., *Tunable, biodegradable gold nanoparticles as contrast agents for computed tomography and photoacoustic imaging.* Biomaterials, 2016. **102**: p. 87-97.
129. Li, M., et al., *Au@MnS@ZnS Core/Shell/Shell Nanoparticles for Magnetic Resonance Imaging and Enhanced Cancer Radiation Therapy.* ACS Applied Materials & Interfaces, 2016. **8**(15): p. 9557-9564.
130. Aioub, M. and M.A. El-Sayed, *A Real-Time Surface Enhanced Raman Spectroscopy Study of Plasmonic Photothermal Cell Death Using Targeted Gold Nanoparticles.* Journal of the American Chemical Society, 2016. **138**(4): p. 1258-1264.
131. Moreira, A.F., et al., *Preparation of end-capped pH-sensitive mesoporous silica nanocarriers for on-demand drug delivery.* European Journal of Pharmaceutics and Biopharmaceutics, 2014. **88**(3): p. 1012-25.
132. Reis, C.A., et al., *Development of gold-core silica shell nanospheres coated with poly-2-ethyl-oxazoline and beta-cyclodextrin aimed for cancer therapy.* Materials Science and Engineering C, 2019. **98**: p. 960-968.
133. Thakor, A.S., et al., *The Fate and Toxicity of Raman-Active Silica-Gold Nanoparticles in Mice.* Science Translational Medicine, 2011. **3**(79): p. 79ra33.

134. Luo, G.-F., et al., *A Triple-Collaborative Strategy for High-Performance Tumor Therapy by Multifunctional Mesoporous Silica-Coated Gold Nanorods.* Advanced Functional Materials, 2016. **26**(24): p. 4339-4350.
135. Xi, D., et al., *Gold nanoparticles as computerized tomography (CT) contrast agents.* RSC Advances, 2012. **2**(33): p. 12515-12524.
136. Wang, Z., et al., *Gemcitabine-loaded gold nanospheres mediated by albumin for enhanced anti-tumor activity combining with CT imaging.* Materials Science and Engineering: C, 2018. **89**: p. 106-118.
137. Kobayashi, Y., et al., *X-ray imaging technique using colloid solution of Au/silica core-shell nanoparticles.* Journal of Nanostructure in Chemistry, 2013. **3**(1): p. 62.
138. Gonçalves, A.S.C., et al., *Strategies to improve the photothermal capacity of gold-based nanomedicines.* Acta Biomaterialia, 2020.
139. Ramasamy, M., J.H. Lee, and J. Lee, *Development of gold nanoparticles coated with silica containing the antibiofilm drug cinnamaldehyde and their effects on pathogenic bacteria.* Int J Nanomedicine, 2017. **12**: p. 2813-2828.
140. Moreira, A.F., et al., *Development of poly-2-ethyl-2-oxazoline coated gold-core silica shell nanorods for cancer chemo-photothermal therapy.* Nanomedicine, 2018. **13**(20): p. 2611-2627.
141. O'Brien, J., et al., *Investigation of the Alamar Blue (resazurin) fluorescent dye for the assessment of mammalian cell cytotoxicity.* (0014-2956 (Print)).
142. Barros, A.S., et al., *Comparative study of the therapeutic effect of Doxorubicin and Resveratrol combination on 2D and 3D (spheroids) cell culture models.* International Journal of Pharmaceutics, 2018. **551**(1-2): p. 76-83.
143. de Melo-Diogo, D., et al., *Combinatorial delivery of Crizotinib-Palbociclib-Sildenafil using TPGS-PLA micelles for improved cancer treatment.* European Journal of Pharmaceutics and Biopharmaceutics, 2014. **88**(3): p. 718-29.
144. Li, X., et al., *Systematic combination screening reveals synergism between rapamycin and sunitinib against human lung cancer.* Cancer Letters, 2014. **342**(1): p. 159-166.
145. Rodrigues, C.F., et al., *Optimization of gold core-mesoporous silica shell functionalization with TPGS and PEI for cancer therapy.* Microporous and Mesoporous Materials, 2019. **285**: p. 1-12.
146. Kalender, Y., M. Yel, and S. Kalender, *Doxorubicin hepatotoxicity and hepatic free radical metabolism in rats: The effects of vitamin E and catechin.* Toxicology, 2005. **209**(1): p. 39-45.
147. Fitzgerald, K.A., et al., *A novel, anisamide-targeted cyclodextrin nanoformulation for siRNA delivery to prostate cancer cells expressing the sigma-1 receptor.* International Journal of Pharmaceutics, 2016. **499**(1): p. 131-145.
148. Li, J., Y. Yang, and L. Huang, *Calcium phosphate nanoparticles with an asymmetric lipid bilayer coating for siRNA delivery to the tumor.* Journal of Controlled Release, 2012. **158**(1): p. 108-114.
149. Wang, L., et al., *Development of anisamide-targeted PEGylated gold nanorods to deliver epirubicin for chemo-photothermal therapy in tumor-bearing mice.* Int J Nanomedicine, 2019. **14**: p. 1817-1833.
150. Aydar, E., et al., *The expression and functional characterization of sigma (σ) 1 receptors in breast cancer cell lines.* Cancer Letters, 2006. **242**(2): p. 245-257.
151. Deng, C., et al., *A biodegradable triblock copolymer poly(ethylene glycol)-b-poly(l-lactide)-b-poly(l-lysine): Synthesis, self-assembly, and RGD peptide modification.* Polymer, 2007. **48**(1): p. 139-149.

152. Xu, F.J., et al., *Spatially well-defined binary brushes of poly(ethylene glycol)s for micropatterning of active proteins on anti-fouling surfaces.* Biosensors and Bioelectronics, 2008. **24**(4): p. 773-780.
153. Chieng, B.W., et al., *Poly(lactic acid)/Poly(ethylene glycol) Polymer Nanocomposites: Effects of Graphene Nanoplatelets.* Polymers, 2014. **6**(1).
154. Fröhlich, E., *The role of surface charge in cellular uptake and cytotoxicity of medical nanoparticles.* International journal of nanomedicine, 2012. **7**: p. 5577-5591.